Article:
Mishra, B, Shoenfelt, E, Yu, Q et al. (3 more authors) (2017) Stoichiometry of mercury-thiol complexes on bacterial cell envelopes. Chemical Geology, 464. pp. 137-146. ISSN 0009-2541

https://doi.org/10.1016/j.chemgeo.2017.02.015

Stoichiometry of mercury-thiol complexes on bacterial cell envelopes

Bhoopesh Mishra[1*†], Elizabeth Shoenfelt[2], Qiang Yu[3], Nathan Yee[4],

Jeremy B. Fein[3], Satish C.B. Myneni[2*]

[1]Physics Department, Illinois Institute of Technology, Chicago, Illinois, USA

[2]Department of Geosciences, Princeton University, Princeton, New Jersey, USA

[3]Department of Civil Engineering & Geological Sciences, University of Notre Dame, Notre Dame, Indiana, USA

[4]Department of Environmental Sciences, Rutgers University, New Brunswick, New Jersey, USA

Keywords: Hg, speciation, stoichiometry, bacteria, thiols, XANES, EXAFS, cell envelope, potentiometric titration, qBBR

[*]Co-corresponding authors. Email: (bmishra3@iit.edu); (smyneni@princeton.edu)
[†]Present address: School of Chemical and Process Engineering, University of Leeds, Yorkshire, UK.

Abstract

We have examined the speciation of Hg(II) complexed with intact cell suspensions (10^{13} cells L^{-1}) of *Bacillus subtilis*, a common gram-positive soil bacterium, *Shewanella oneidensis* MR-1, a facultative gram-negative aquatic organism, and *Geobacter sulfurreducens*, a gram-negative anaerobic bacterium capable of Hg-methylation at Hg(II) loadings spanning four orders of magnitude (120 nM to 350 µM) at pH 5.5 (±0.2). The coordination environments of Hg on bacterial cells were analyzed using synchrotron based X-ray Absorption Near Edge Structure (XANES) and Extended X-ray Absorption Fine Structure (EXAFS) spectroscopy at the Hg L_{III} edge. The abundance of thiols on intact cells was determined by a fluorescence-spectroscopy based method using a soluble bromobimane, monobromo(trimethylammonio)bimane (qBBr) to block thiol sites, and potentiometric titrations of biomass with and without qBBr treatment. The chemical forms of S on intact bacterial cells were determined using S k-edge XANES spectroscopy.

Hg(II) was found to complex entirely with cell bound thiols at low Hg:biomass ratios. For *Bacillus subtilis* and *Shewanella oneidensis* MR-1 cells, the Hg-S stoichiometry changed from Hg-S_3 to Hg-S_2 and Hg-S (where 'S' represents a thiol site such as is present on cysteine) progressively as the Hg(II) loading increased on the cells. However, *Geobacter sulfurreducens* did not form Hg-S_3 complexes. Because the abundance of thiol was highest for *Geobacter sulfurreducens* (75 µM/g wet weight) followed by *Shewanella oneidensis* MR-1 (50 µM/g wet weight) and *Bacillus subtilis* (25 µM/g wet weight), the inability of Hg(II) to form Hg-S_3 complexes on *Geobacter sulfurreducens* suggests that the density and reactivity of S-amino acid containing cell membrane proteins on *Geobacter sulfurreducens* are different from those of *Bacillus subtilis* and *Shewanella oneidensis* MR-1. Upon saturation of the high affinity thiol sites at higher Hg:biomass ratios, Hg(II) was found to form a chelate with α-hydroxy carboxylate anion. The stoichiometry of cell envelope bound Hg-thiol complexes and the associated abundance of thiols on the cell envelopes provide important insights for understanding the differences in the rate and extent of uptake and redox transformations of Hg in the environment.

1.0 Introduction

Mercury is a common contaminant found in many terrestrial and aquatic systems, and its bioaccumulation in organisms, including humans, is a major environmental concern (Mergler et al, 2007). The solubility, speciation, toxicity and the ultimate fate of Hg within aquatic ecosystems is dependent on a large number of chemical and biological variables (Morel et al., 1998; Barkay and Schaefer, 2001). In aquatic systems, Hg solubility is high under oxygen-rich acidic conditions but it is significantly inhibited under anoxic sulfide-rich waters (Martell and Smith, 1974). The Hg-sulfide complexes are among the strongest complexes of all known Hg inorganic and organic complexes in the aquatic environment (Carty and Malone, 1979). While the presence of sulfides in aqueous systems can induce precipitation of Hg in the form of insoluble amorphous and crystalline HgS, stable aqueous polysulfide complexes and nanoparticles can also enhance the solubility and transport of Hg. In addition, inorganic ligands (e.g. Cl^-), and mono- (e.g. cysteine) and poly-dentate (e.g. citrate, catechols) organic ligands can also enhance the solubility of Hg by forming stable aqueous complexes. Complex organic ligands, such as natural organic matter (NOM), also form stable Hg-NOM complexes through thiol (SH), and carboxyl binding (Xia et al., 1999; Haitzer et al., 2002; Khwaja et al., 2006; Skyllberg et al., 2005; Skylberg 2008; Nagy et al., 2011; Hesterberg et al., 2001). Because dissolved organic matter (DOM) is the main source of reduced cysteine residues in natural waters, Hg complexation with DOM is thought to control the speciation, solubility, mobility, and toxicity of Hg in the aquatic environment (Loux, N., 1998; Ravichandran, M., 2004), indirectly affecting the rate and extent of Hg-methylation (Ravichandran, M., 2004).

One of the key biogeochemical transformations of interest is the role of microorganisms in converting Hg to methyl mercury. While the geochemical factors that control Hg methylation in terrestrial and aquatic systems are poorly understood, it has been shown that the concentration of Hg bioavailable to Hg-methylating bacteria is strongly affected by binding to cysteine residues (Skyllberg et al., 2006), and the extent of Hg(II) uptake and Hg-methylation is significantly influenced by the presence of Hg-cysteine complexes in aqueous solutions (Schaefer and Morel, 2009; Schaefer et al., 2011; Thomas et al., 2014; Lin et al., 2015).

Thiol sites within bacterial cell envelopes have been shown to control the fate and transport of Hg by providing high-affinity binding sites (Mishra et al., 2011), and mediating redox transformations (Colombo et al., 2013; Hu et al., 2013; Colombo et al., 2014). Certain bacterial strains such as *Geobacter sulfurreducens* PCA can function both as a reductant and as an adsorbent for Hg(II) at different cell biomass to Hg ratios (Hu et al., 2013), with adsorption being the dominant mechanism at low Hg:biomass ratios. Sorption of Hg(II) to cell envelope sites has been thought to serve as a "sink" for Hg(II) that restricts transport into the cytoplasm, thus lowering the bioavailability of Hg(II) (Graham et al., 2012). Recent studies indicate that in addition to gene expression and regulation, cell envelope chemistry is likely an important driver for cross-species differences in Hg methylation rates (Graham et al., 2012). Furthermore, reactivity of thiols towards Hg(0), resulting in thiol mediated passive microbial oxidation of Hg(0), has been recently reported (Colombo et al., 2013; Colombo et al., 2014). Since physicochemical sorption of Hg(0) to reactive thiol sites has been hypothesized as the first step in Hg(0) oxidation by dissolved organic matter (Gu et al., 2011; Zheng et al., 2012), differences in passive Hg(0) oxidation rates by different bacterial strains could be explained by the reactivity

and density of thiols present on the cell envelopes of corresponding bacterial strains (Colombo et al., 2014).

In spite of the significance of Hg-thiol complexation on cell envelopes, the speciation and stability of thiol-bound Hg on cell envelopes remains largely unknown. X-ray-based spectroscopy investigations could provide definitive information regarding the nature of Hg(II) interactions with bacterial cell envelopes. To date, studies have been primarily limited to showing the complexation of Hg with high (thiol) and low (carboxyl) affinity sites on cell envelopes (Mishra et al., 2011; Dunham-Cheatham et al., 2014; Dunham-Cheatham et al., 2015). Although recent studies have shown variations of the stoichiometry of thiol bound Hg on the cell, they are either qualitative using a XANES fingerprinting technique (Thomas et al., 2014) or limited in scope (Thomas et al., 2016). Similar to the complexation of Hg with NOM, Hg-thiol complexes within bacterial cell envelopes may exhibit a range of stoichiometries as a function of Hg loading conditions. The speciation and stability of such cell envelope bound Hg-thiol complexes may in fact control the overall fate and bioavailability of Hg in aquatic systems. This study provides direct evidence for systematic changes in the stoichiometry of Hg-thiol complexes on bacterial cell envelopes for three different bacterial species.

For an in-depth evaluation of the speciation of Hg bound to cell envelopes and the stoichiometry of Hg-thiol complexes under ambient conditions, we selected three distinct classes of bacteria: *Bacillus subtilis*, a common Gram-positive soil bacterium, *Shewanella oneidensis* MR-1, a facultative Gram-negative aquatic organism, and *Geobacter sulfurreducens*, a Gram-negative anaerobic bacterium capable of methylating mercury; and exposed the intact cell suspensions (10^{13} cells L^{-1}, or ~2 g L^{-1} of wet mass) to different concentrations of dissolved Hg(II) (120 nM to 350 µM) at pH 5.5 (±0.2). The structure and coordination environments of Hg on the bacterial cells were analyzed using synchrotron-based X-ray Absorption Near Edge Structure (XANES), and Extended X-ray Absorption Fine Structure (EXAFS) spectroscopy at the Hg L_{III} edge. The abundance of thiols on the intact cells was directly determined by a fluorescence-spectroscopy-based method, using a soluble bromobimane, monobromo(trimethylammonio)bimane (qBBr), and was further verified by the change in total thiol concentrations on intact cells using potentiometric titrations of biomass with and without qBBr treatment. The chemical forms of S on intact bacterial cells were determined using S k-edge XANES spectroscopy.

2.0 Materials and Methods

2.1 Bacterial Growth Conditions

Bacillus subtilis and *Shewanella oneidensis* MR-1 cells were cultured and prepared aerobically following the procedures outlined elsewhere (Borrok et al., 2007). Briefly, cells were maintained on agar plates consisting of trypticase soy agar with 0.5% yeast extract added. Cells for all experiments were grown by first inoculating a test-tube containing 3 mL of trypticase soy broth with 0.5% yeast extract, and incubating it for 24 h at 32 °C. The 3 ml bacterial suspension was then transferred to a 1 L volume of trypticase soy broth with 0.5% yeast extract for another 24 h on an incubator shaker table at 32 °C. Cells were pelleted by centrifugation at 8100g for 5 min, and rinsed 5 times with 0.1 M $NaClO_4$.

Geobacter sulfurreducens cells were cultured and prepared using a different procedure than described above. Cells were maintained in 50 mL of anaerobic freshwater basal media (ATCC 51573) at 32 ºC (Lovely and Phillips, 1988). Cells for all experiments were grown by first inoculating an anaerobic serum bottle containing 50 mL of freshwater basal media, and incubating it for 5 days at 32 ºC. Cells were pelleted by centrifugation at 8100g for 5 minutes, and rinsed 5 times with 0.1 M $NaClO_4$ stripped of dissolved oxygen by bubbling a 85%/5%/10% $N_2/H_2/CO_2$ gas mixture through it for 30 minutes. After washing, the three types of bacteria used in this study were then pelleted by centrifugation at 8100g for 60 minutes to remove excess water to determine the wet mass so that suspensions of known bacterial concentration could be created.

Experimental conditions for all the cell cultures described above represent the early exponential phase of the bacterial growth curves.

2.2 Hg Adsorption Experiments

A 200 ppm parent solution of Hg^{2+} in 0.1 M $NaClO_4$ was prepared from a commercially-supplied 1000 ppm Hg in nitric acid reference solution, which was adjusted to pH 3.0 by adding aliquots of 1 M NaOH. Appropriate amounts of the Hg(II) parent solution were added to achieve the desired Hg(II) and bacterial concentrations (Table S1). The concentration of the bacterial suspensions was 2 g L^{-1} (~ 10^{13} cell L^{-1}) for all of the experiments in this study. The pH of each system was adjusted to 5.5 (± 0.2) using small aliquots of 1 M HNO_3 or NaOH, and the systems were allowed to react for two hours on a shaker at room temperature (22 °C). Since surface waters exposed to the atmosphere have a pH of approximately 5.6 due to the dissolution of carbon dioxide into the water, we chose to work at pH 5.5 to make our results relevant to environmental and geochemical systems. Metal adsorption on bacterial cell surfaces have been previously conducted at similar pH conditions (Boyanov et al., 2003; Claessens and Van Cappellen, 2007; Wei et al., 2011). In addition, we conducted experiments at pH 5.5 to exclude potential effects of insoluble Hg-hydroxide formation which are highly favorable at alkaline pH conditions. pH was monitored every 30 min, and adjusted as required. After 2 h of reaction, the suspensions were centrifuged, and the bacterial pellet from each experiment was retained for XAFS analysis. The supernatant was filtered (0.45 μm) using nylon membranes (Millipore filter), acidified, and analyzed for dissolved Hg(II) by inductively coupled plasma-optical emission spectroscopy (ICP-OES; Perkin-Elmer). Filtering supernatant using Fluoropore PTFE membranes filter (0.45 μm) did not result in appreciable change in the concentration of Hg in supernatant.

Previous experiments (Fowle and Fein, 2000) have demonstrated the reversibility of metal binding reactions under similar experimental conditions, strongly suggesting that the metals are not internalized during the course of the experiments.

2.3 Hg XAS Measurements and Data Analysis

Hg L_{III} edge X-ray absorption near edge structure (XANES) and extended X-ray absorption fine-structure spectroscopy (EXAFS) measurements were performed at the MRCAT sector 10-ID beamline (Segre et al., 2000), Advanced Photon Source, at Argonne National Laboratory. The continuous scanning mode of the undulator was used with a step size and integration time of 0.5 eV and 0.1 s per point, respectively, in order to decrease the radiation exposure during a single scan. In addition, the measurements were conducted at different spots on the sample to further decrease the time of exposure. XANES spectroscopy, which is sensitive

to chemical changes in the sample, was constantly monitored for any possible radiation damage. Successive XANES scans did not show any beam induced changes in any of the samples studied (data not shown).

Hg XANES and EXAFS measurements and the data analysis approach for this study were similar to those previously published by our group (Mishra et al., 2011; Pasakarnis et al., 2013; Dunham-Cheatham et al., 2014; Dunham-Cheatham et al., 2015). The data were analyzed using the methods described in the UWXAFS package (Stern et al., 1995). Energy calibration between different scans was maintained by measuring a Hg/Sn amalgam, prepared as described elsewhere (Harris et al., 2003), on the reference chamber concurrently with the fluorescence measurements of the biomass-bound Hg samples. The inflection point of the Hg L_{III} edge (12.284 KeV) was used for calibration of the scans. Data processing and fitting was done with the programs ATHENA and ARTEMIS (Ravel and Newville, 2005). The data range used for Fourier transforming the *k* space data was 2.3–9.8 $Å^{-1}$, except in the case of the two lowest Hg concentration samples where 2.3–8.2 $Å^{-1}$ was used due to poor data quality. The Hanning window function was used with a dk of 1.0 $Å^{-1}$. Fitting of each spectrum was performed in *r*-space, from 1.2–3.2 Å, with multiple *k*-weighting (k^1, k^2, k^3) unless otherwise stated. Lower χ_v^2 (reduced chi square) was used as the criterion for inclusion of an additional shell in the shell-by-shell EXAFS fitting procedure.

2.4 Hg XAS Standards

Crystalline powder standards (cinnabar [red HgS] and mercuric acetate) were measured and used to calibrate the theoretical calculations against experimental data. Data from the standards were analyzed to obtain the $S0^2$ parameter, where $S0^2$ is the value of the passive electron reduction factor used to account for the many body effects in EXAFS. By fixing the value of S and O atoms to 2 in cinnabar and mercuric acetate, we obtained $S0^2$ values of 1.02 ± 0.05 and 0.98 ± 0.03, respectively. Hence, we chose to set the value of $S0^2$ to be 1.0 for all the samples. Fitting of the powder standards to their known crystallographic structure (cinnabar and mercuric acetate) reproduced the spectral features in the entire fitting range (1.0–4.2 Å) and the fitting parameters were in agreement with previously reported values (Almann, R., 1973; Manceau and Nagy, 2008). Only the paths necessary to model the solid standards were used for fitting the solution standards and the unknown Hg samples.

In addition to crystalline powder standards, solution-phase standards (Hg^{2+}, Hg-cysteine, and Hg-acetate) were also measured as solution standards in order to provide a better representation of aqueous metal speciation than crystalline powder standards. Aqueous Hg^{2+} and Hg-cysteine standards were prepared from high purity 5mM Hg^{2+} in 5% HNO_3 bought from GFS Chemicals. Hydrated Hg^{2+} was adjusted to pH 2.0 for measurement by adding appropriate amounts of 5 M NaOH. A Hg-cysteine standard was prepared by adding cysteine to 5mM Hg^{2+} in 5% HNO_3 in a Hg:ligand ratio of 1:100. The pH of the Hg-cysteine solution was adjusted to 5.0 and 8.0 by adding appropriate amounts of 5 or 1 M NaOH to obtain solutions with predominantly Hg-$(cysteine)_2$ and Hg-$(cysteine)_3$ present, respectively. It must be emphasized that solution species are almost always a mixture of different Hg-cysteine species. Although the presence of small fractions (less than 10%) of other stoichiometries of Hg-cysteine complexes in the Hg-$(cysteine)_2$ and Hg-$(cysteine)_3$ standards cannot be ruled out, comparison of the Hg-S bond lengthes determined using EXAFS modeling of these standards with published values was used to validate their stoichiometries. The Hg-acetate standard was prepared by adding mercuric-

acetate salt to ultrapure water and the pH of this solution was adjusted to 5.0 by adding appropriate amounts of 1 and 5 M NaOH. The best fit values of the Hg-(cysteine)$_2$, Hg-(cysteine)$_3$, and Hg-acetate solution standards were used as the initial values of the corresponding variables for fitting the unknown Hg biomass samples.

2.5 S XANES Measurement and Analysis

Sulfur K-edge XANES spectra for biomass samples were acquired at the National Synchrotron Light Source (NSLS, Brookhaven) on beamline X19A using a PIPS detector in fluorescence detection mode. At X19A, signal from higher order harmonics was removed by detuning the monochromator to 70% of the maximum beam flux at 2472.0 eV. An energy calibration was performed by setting the first peak in the spectrum of sodium thiosulfate salt ($Na_2S_2O_3$), corresponding to the thiol S, to 2469.2 eV. XANES spectra were typically measured between 2450 and 2500 eV. Step sizes in the near-edge region (2467-2482 eV) were 0.08 eV, and 0.2 eV in pre- and post- edge regions.

2.6 Thiol Quantification with qBBr Titrations

The concentration of bacterial cell envelope thiols was quantified by reacting a known cell density with increasing concentrations of qBBr in water and detecting fluorescence with a Photon Technology International Quantamaster fluorometer. The qBBr was purchased from Sigma-Aldrich and Toronto Research Chemicals. When excited at 380 nm, the qBBr-thiol complex has a maximum emission at 470 nm. When emission intensity is plotted against qBBr concentration, the thiol concentration in the cell suspension is evident by a decrease in the slope of intensity per qBBr concentration to the background level (the fluorescence of qBBr in water). Optical density of the cells in water at 260 nm was below the detection limit of the spectrophotometer, indicating low DNA concentrations which could result from cell lysis. Further details about this method are provided elsewhere (Joe-Wong et al., 2012).

2.7 Thiol Determination with Potentiometric Titrations

The change in total site concentrations on cell envelopes determined by potentiometric titrations of biomass with and without qBBr treatment was used as a direct measure of the thiol site concentration. Details of the procedure and modeling approach are given in Yu et al. (2014). Briefly, bacterial suspensions were allowed to react for 2 h with a qBBr-bearing solution with a qBBr:bacteria ratio of 130 µmol qBBr/g (wet biomass), followed by three rinses. Potentiometric titrations in de-gassed 0.1 M NaCl were conducted under a headspace of N_2 gas to exclude atmospheric CO_2 and each suspension was stirred continuously.

3.0 Results

3.1 Hg adsorption

Hg adsorption on the three bacterial species over four orders of magnitude is shown in table S1. Hg was found to be below the detection limit of ICP under low aqueous Hg concentration regime suggesting that Hg adsorbs strongly onto bacterial cells, with nearly complete removal of Hg from aqueous solutions under these experimental conditions. Increase in aqueous Hg concentration resulted in lower fraction of adsorbed Hg for all the three species examined. These trends demonstrate that the total number of deprotonated sites around pH 5.5 are similar for all the three species. Previous study has shown the transition from reduction of Hg

to adsorption of Hg associated with biomass concentrations of 10^{10} to 10^{13} cells/L (Hu et al., 2013). Since the experiments presented here contain 10^{13} cells/L, we rule out reduction of Hg in our study. It should also be noted that a rigorous Hg mass balance has not been presented here. Mass balance is not relevant for this study and does not affect any of our results or conclusions because our work focuses on elucidating the mechanism of complexation of Hg with cell membranes.

3.2 Qualtitative XAS Analysis of Hg Standards

The XANES spectra for the solution-phase Hg^{II} standards (Hg^{2+}, Hg-acetate, Hg-(cysteine)$_2$, and Hg-(cysteine)$_3$) are shown in Figure 1. The XANES spectra of these three standards have significantly different spectral features (Figure 1): Hg^{2+} is out of phase with the rest of the standards presented here and has a distinct peak at 12310 eV; Hg-acetate has a pronounced pre-edge feature at about 12285 eV; the Hg-(cysteine)$_2$ complex exhibits a much smaller pre-edge feature at 12290 eV than the Hg-acetate complex and exhibits another shoulder at 12300 eV; the Hg-(cysteine)$_3$ has a further smaller pre-edge peak (with 12290 and 12300 eV shoulder missing) and has a distinctly different post-edge shape which is easily distinguishable from the Hg-(cysteine)$_2$ standard and the rest of the standards presented here. Comparison of the XANES spectra for the Hg-(cysteine)$_2$ and Hg-(cysteine)$_3$ standards can be seen in Figure S1a.

A shift to higher radial distance in the first peak of the Fourier transformed (FT) data for the Hg–(cysteine)$_2$ spectrum relative to the Hg-acetate standard spectrum, arising from the bonding of Hg to sulfur in the first shell as opposed to bonding to oxygen, can be seen in Figure 2. The longer distance of the first peak for the Hg–(cysteine)$_2$ spectrum compared with the Hg-acetate standard is concomitant with a larger amplitude of the FT EXAFS data for the Hg–(cysteine)$_2$ as expected from a heavier backsctetter (Figure 2). In addition, the radial distance for the first peak of the Hg-(cysteine)$_3$ standard is longer than that of the Hg-(cysteine)$_2$ standard, also evident in the phase shift of the Hg-(cysteine)$_3$ standard towards lower k value (Figure S1). However, the Hg-(cysteine)$_3$ standard has a smaller amplitude than the Hg-(cysteine)$_2$ standard because a distorted trigonal planer structure has a larger structural disorder associated with it compared to the linear Hg-(cysteine)$_2$ complex. Hence, careful comparison of the XANES and EXAFS data from the Hg biomass samples can be used to determine whether the Hg associated with biomass is bound to the biomass through Hg –carboxyl or –thiols, and the stoichiometry of Hg:thiol complexes can also be determined from the data.

3.3 Quantitative XAS Analysis of Hg Standards

Best fit values resulting from EXAFS analysis of the solution standards are given in Table 1. The aqueous Hg^{2+} standard was best fit with Hg being bound to 6.12 (± 0.65) O atoms at 2.30 (± 0.01) Å, which is consistent with an octahedral coordination geometry of a hydrated Hg^{2+} ion (Richens, D. T., 1997). Hg-acetate was best fit with 1.78 (± 0.32) O atoms at 2.06 (± 0.01) Å in the first shell. The number of C atoms, which was fixed to be equal to the number of O atoms in the first shell, was found at 2.83 (± 0.01) Å, consistent with the crystal structure of mercuric acetate (Almann, R., 1973). The Hg-(cysteine)$_2$ solution was best fit with 1.88 (± 0.21) S atoms at 2.32 (± 0.01) Å in the first shell, which indicates complexation of Hg with two cysteine moieties (Manceau and Nagy, 2008). Inclusion of C atoms did not lower the χ_v^2 (Stern et al., 1995) value significantly enough to justify the addition of another shell. The Hg-(cysteine)$_3$ solution was best fit with 2.82 (± 0.32) S atoms at 2.49 (± 0.01) Å in the first shell.

Published literature suggests that a Hg-S bond distance of 2.49 Å is representative of the Hg-S_3 complex, but could possibly include small components of Hg-S_2 and Hg-S_4 complexes as well (Manceau and Nagy, 2008; Warner and Jalilehvand, 2016). In summary, the fitting parameters for the solution standards reported in this study are in good agreement with previously published values (Xia et al., 1999; Qian et al., 2002; Skyllberg et al., 2006; Mishra et al., 2011; Thomas et al., 2016).

3.4 Hg(II) complexation with biomass

The following conclusions can be drawn concerning Hg binding onto the biomass samples, and the descriptions in this section describe the evidence for these conclusions in more detail. Hg(II) was found to complex entirely with thiols at low Hg:biomass ratios. The Hg coordination changed from Hg-S_3 to Hg-S_2 and Hg-S progressively as the Hg(II) loading increased on the cells. These Hg-S_n (where n=1-3) bacterial surface complexes also exhibit different Hg-S bond distances (2.3-2.5 Å) with the longest in the Hg-S_3 complex, consistent with published literature (Manceau and Nagy, 2008). Upon saturation of the high affinity thiol sites at higher Hg:biomass ratios, Hg^{2+} was found to form a chelate with carboxyl and a neighboring hydroxyl (α-hydroxy carboxylate anion) based on the measured Hg-O and Hg-C distances (Table 1). Such α-hydroxy carboxylic acids have been reported to occur abundantly within cell envelopes (Wei et al., 2004). While all the species exhibit strong affinities for Hg^{2+} at low Hg:biomass ratios, the differences in Hg-S stoichiometry between the cell envelopes of *S. oneidensis* MR-1 and *G. sulfurreducens* is noteworthy.

3.4.1 Hg(II) complexation with *Shewanella oneidensis* MR-1

Figure 1a shows the XANES data of Hg(II) complexed to *Shewanella oneidensis* MR-1 biomass as a function of Hg loading. Comparision of the XANES spectra for the Hg-biomass samples with the Hg standards suggests that the transition from thiol to carboxyl functional groups takes place around 50 µM Hg(II). A systematic change in the amplitide and phase shift of oscillations in the k^2-weighted χ(k) data of the Hg-biomass samples can be seen in Figure 2a. Hg is complexed exclusively via thiols in samples containing less than 50 µM Hg(II), while Hg is complexed exclusively via carboxyl functional groups in samples containing more than 50 µM Hg(II). Samples containing 0.5 µM or less Hg(II) have a spectral signature of Hg-(cysteine)$_3$ binding. The FT EXAFS data from the biomass samples with 350, 15, and 0.5 µM Hg(II) have spectral features and first shell bond distances similar to the following aqueous Hg standards respectively: Hg-acetate, Hg-(cysteine)$_2$, and Hg-(cysteine)$_3$ (Figure 3a). The differences between the amplitude and bond distances of the 350, 15, and 0.5 µM Hg(II) samples and their similarities with Hg-acetate, Hg-(cysteine)$_2$, and Hg-(cysteine)$_3$ solution standards, respectively, are further illustrated in the real part of the Fourier transforms shown in Figure 3b. Based on bond distances and amplitude of the FT data, the Hg-biomass samples can be divided into three sub-groups: 350-50 µM Hg(II), 25-5 µM Hg(II), and 0.5 µM Hg(II) (Figures 1 and 3). These three sub-groups of biomass samples appears to be dominated by Hg-carboxyl, Hg-(cysteine)$_2$, and Hg-(cysteine)$_3$ binding environments, respectively. The 2.5 µM Hg(II) sample can be well-described by a linear combination of the 0.5 and 5.0 µM Hg(II) biomass samples, suggesting that Hg-(cysteine)$_2$ and Hg-(cysteine)$_3$ coordination environments comprise approximately 58 and 42% (± 5%) of the bound Hg, respectively.

The Hg-biomass data were modelled quantitatively as described above. Best fit values are given in Table 1. The 350 µM Hg(II) data was best fit with 1.65 (± 0.25) O atoms at 2.06 (± 0.01) Å in the first shell. Inclusion of 1.58 (±0.32) C atoms in the second shell resulted in significant improvement of the fit. However, the Hg-C distance for this sample was 3.05 (± 0.02) Å, which is much longer than the Hg-C distance determined for the Hg-acetate solution standard (2.83 ± 0.01 Å). This suggests the formation of a carboxyl with alpha-hydroxy carboxylic acid or a malate type coordination geometry for the biomass samples. The 100 and 50 µM Hg(II) data did not show any appreciable change in the coordination environment, except that the 50 µM Hg(II) data was improved by inclusion of S atoms in the first shell. The coordination number of S was 0.56 (± 0.12), suggesting a small fraction of Hg atoms bound to thiols for this sample. The 25 µM Hg(II) biomass sample was best fit with 1.32 (± 0.21) S atoms at about 2.31 (± 0.01) Å in the first shell. The 15 and 5 µM Hg(II) samples were best fit with ~1.8 (± 0.2) S atoms at about 2.32 (± 0.02) Å in the first shell. The 2.5 µM Hg(II) sample was best fit as a linear combination of Hg-$(cysteine)_2$ and Hg-$(cysteine)_3$ coordination environments, with ~2.2 (± 0.3) S atoms at about 2.44 (± 0.01) Å in the first shell. The 0.5 µM Hg(II) sample was mostly Hg-$(cysteine)_3$ with 2.96 (± 0.25) S atoms at 2.51(± 0.01) Å. Inclusion of an O/N atom in the first shell or a C atom in the second shell did not result improve the fit for the samples containing 25 µM Hg(II) or less.

A recent study has suggested the formation of a Hg-S_4 complex on *E. coli* cells under actively metabolizing conditions (Thomas et al., 2016). While the experimental conditions studied by Thomas et al. (2016) are different from those in this study, formation of Hg-S_4 complex on bacterial cells is unlikely at circumneutral pH conditions because Hg-$(cysteine)_4$ solution complexes are formed only under highly alkaline conditions (Warner and Jalilehvand, 2016). Thomas et al. (2016) also conducted XAS measurements at very low temperatures, which can induce the formation of tetrathiolate complexes (Nagy et al., 2011). Further, biochemical considerations support the existence of Hg-$(cysteine)_3$ but not Hg-$(cysteine)_4$ complexes on cell envelopes (Cheesman et al., 1988).

Although it is possible that Hg goes on to N (amines) sites after saturating S (thiols) sites which constitute a small number of sites and quickly get masked by transition of Hg to O (carboxyl) sites which are much more abundant, we do not see any evidence for the same. Hg XANES for Hg-histidine aqueous solution does not resemble Hg-biomass samples at high Hg loadings (figure S2).

3.4.2 Hg(II) complexation with *Bacillus subtilis* and *Geobacter sulfurreducens*

A similar appraoch was adopted to model the Hg-biomass data for the *B. subtilis* and *G. sulfurreducens* samples. Trends similar to the *S. oneidensis* MR-1 data can be seen in the k^2-weighted $\chi(k)$ EXAFS data of the Hg biomass samples for *B. subtilis* and *G. sulfurreducens* (Figure 3). Figures S3a and S3b show the XANES and figures S4a and S4b show the data and fit of the EXAFS FT magnitude for *B. subtilis* and *G. sulfurreducens* samples, and the best fit values for the Hg EXAFS modeling are provided in Table 1.

In the case of *B. subtilis*, the 350, 100, and 75 µM Hg(II) samples were modeled exclusively as Hg-carboxyl binding, and did not exhibit any signature of thiol complexation of Hg. The 25 and 15 µM samples for *B. subtilis* were found to have some Hg-thiol comlexation

with a larger fraction of the Hg atoms complexed with carboxyl groups, similar to the 50 µM Hg(II) sample for *S. oneidensis* MR-1. The *B. subtilis* samples with 5.0, 2.5, and 0.5 µM Hg(II) were modeled with 1.80 ± 0.2, 1.95 ± 0.3, and 2.26 ± 0.3 S atoms at 2.32 ± 0.01, 2.33 ± 0.01, and 2.45 ± 0.01 respectively. The 5.0 and 2.5 µM Hg(II) samples exhibit Hg-(cysteine)$_2$ coordination environment. The 0.5 µM Hg sample for *B. subtilis* is a combination of Hg-(cysteine)$_2$ and Hg-(cysteine)$_3$ coordination environments, similar to the 2.5 µM Hg sample for *S. oneidensis* MR-1. In summary, the stoichiometry of Hg(II) on Gram-positive *B. subtilis* cells follows the same trend as we observed for the Gram negative *S. oneidensis* MR-1 cells. However, the transition from carboxyl to thiol and Hg-(cysteine)$_2$ to Hg-(cysteine)$_3$ complexation takes place at lower Hg(II) concentrations for the *B. subtilis* samples. Differences in the abundance of thiols within the cell envelopes of *B. subtilis* and *S. oneidensis* MR-1 (see below) are likely to explain the offset in Hg(II) concentration between these two species at which the transition in binding environment occurs.

The Hg EXAFS analysis of the 75 µM Hg sample for *G. sulfurreducens* indicated that a small fraction of Hg was bound to thiol sites, with a majority of the Hg bound to carboxyl, which was similar to what we observed for the 50 and 25 µM Hg samples for *S. oneidensis* MR-1 and for *B. subtilis*, respectively. This observation suggests an offset in the loading of Hg(II) at which Hg binding transitions from predominantly carboxyl to thiol for *G. sulfurreducens* compared with *S. oneidensis* MR-1 and *B. subtilis*. However, the offset in Hg(II) loading in the case of *G. sulfurreducens* is opposite to that of *B. subtilis.* Since the signature of Hg-(cysteine)$_3$ binding was observed for the *B. subtilis* samples at lower Hg(II) concentration than for the *S. oneidensis* MR-1 samples, it would be expected that the stoichiometry of Hg(II) complexation with *G. sulfurreducens* cells would transition from Hg-(cysteine)$_2$ to Hg-(cysteine)$_3$ at higher Hg(II) concentrations than was observed for *S. oneidensis* MR-1. Nevertheless, Hg-S bond distances and coordination numbers for *G. sulfurreducens* changed only slighty from 2.32 ± 0.01 Å and 1.70 ± 0.2 for the 25 µM Hg sample to 2.38 ± 0.01 Å and 2.24 ± 0.2 for the 0.5 µM Hg sample, suggesting a lack of formation of Hg-(cysteine)$_3$ stoichiometry within the *G. sulfurreducens* cell envelope (Figures 2c and 2d). This result is somewhat surprising, and could provide important clues about Hg bioavailability for intracellular biochemical process (more below).

3.5 Sulfur XANES

Although the S K-edge XANES spectra were collected on a large number of standards, in this study we have broken down the S species into three main categories for the sake of clarity: reduced S (below 2472 eV), sulfoxide S (near 2473.5 eV), and oxidized S (above 2476.5 eV). Cysteine, dimethyl sulfoxide (DMSO), sodium dodecylsulfate (NaDS), and sodium laurel sulfate Na_2SO_4 standards are shown in Figure 4a. More extensive model libraries that include XANES spectra of organic and inorganic S compounds are available in the literature (Vairavamurthy A., 1998; Myneni, S. C. B., 2002). As seen in Figure 4a, species with very different S oxidation states such as cysteine, sulfoxide, and ester sulfate are easily resolved in the XANES spectrum. Within these three energy ranges, however, resolution becomes more difficult. Reduced sulfur species, including thiols, sulfides, polysulfides, and thiophenes, all have white-line features occurring between 2469 and 2472 eV. S K-edge XANES shows sensitivity to changes in the electronic environment of the sulfur absorber. For example, perturbation in the electron donating ability of the organic moiety changes the energy positions of pre-edge features by affecting the effective nuclear charge on the sulfur atom (Szilagyi and Schwab, 2005).

The S-XANES spectrum of the *S. oneidensis* MR-1 cells cultured under different conditions (aerobic, nitrate, fumarate) and titrated to pH values ranging from pH 4 to 8, indicate a high abundance of reduced S groups (e.g. mono-, and disulfide) relative to the oxidized forms of S (e.g., sulfate, sulfonate) (Figure 4b and 4c). However, monosulfides, such as S in methionine and cysteine, exhibit similar spectral features and are hard to distinguish (Vairavamurthy, A., 1998; Xia et al., 1998; Myneni, S. C. B., 2002; Szilagyi and Schwab, 2005; Risberg et al., 2009). Because thiols are known to exhibit stronger interactions with Hg(II) among these reduced monosulfides (or thioether), we conclude that Hg(II) must be interacting with thiols and our Hg-thiol stoichiometry results obtained using Hg XAS are likely independent of experimental pH (except in extreme environments) and cell culturing conditions.

Interaction of Hg(II) with thiols within cell envelopes is also evident from the changes in S XANES spectra as a function of Hg(II) loading. When the bacterial cells were exposed to increasing levels of Hg(II), the pre-edge feature of the S XANES spectra of the cell suspensions indicated gradual changes in S-speciation, corresponding to the deprotonation and subsequent complexation of thiol with Hg^{2+} (Figure S5; Risberg et al., 2009; Szilagyi and Schwab, 2005). The pre-edge feature of the S K-edge XANES data (figure S5) as a function of Hg loading on *S. oneidensis* MR-1 suggests the deprotonation of cysteine at higher Hg loadings (Szilagyi and Schwab, 2005).

3.6 *Thiol Quantification with qBBr Titrations*

qBBr is a large, thiol-sensitive, charged, water-soluble fluorophore molecule, which does not cross the cell envelope, making it an ideal probe for measuring the concentration of thiols within the cell envelope (Joe-Wong et al., 2012; Rao et al., 2014). Our qBBr titrations suggest that the concentration of reactive thiols within the cell envelopes of *B. subtilis, S. oneidensis* MR-1, and *G. sulfurreducens* are 24±2, 49±12, and 240±80 μM/g wet weight cells, respectively. These wet weight values correspond to 120±10, 300±70, and 1000±300 μM/g dry weight cells, respectively (Figure 5a; Table 2). The cell envelope thiol concentrations determined using qBBR fluorophore measurements for *B. subtilis* and *S. oneidensis* MR-1 are in good agreement with published results (Joe-Wong et al., 2012). These results are also in excellent agreement with the Hg EXAFS analyses (described above) showing the transition of Hg speciation from Hg-carboxyl binding to Hg-thiol complexation for *B. subtilis* and *S. oneidensis* MR-1 at approximately 25 and 50 μM Hg(II), respectively. However, thiol concentrations for *G. sulfurreducens* obtained from the qBBr measurements in this study are higher than those recently reported by another study using a similar technique (Rao et al., 2014) and our Hg EXAFS analyses. If thiol concentrations on *G. sulfurreducens* were as small as previously reported (Rao et al., 2014), Hg complexation with thiols would saturate all the thiol sites on *G. sulfurreducens* cells at much lower Hg(II) concentrations, and transition from Hg-thiol coordination environment to Hg-carboxyl interactions at much lower Hg(II) loading. Hence, our Hg EXAFS results do not agree with the thiol quantification on *G. sulfurreducens* either from this study or with those reported previously (Hu et al., 2013; Rao et al., 2014). To resolve these differences another direct measurement of the thiol site concentrations on *G. sulfurreducens* cells was conducted using potentiometric titrations with and without qBBr treatment of *G. sulfurreducens* cells.

3.7 Thiol Determination with Potentiometric Titrations

Potentiometric titrations (see Yu et al., 2014 for details) were performed on *G. sulfurreducens* with and without qBBr treatment to resolve the difference of over two orders of magnitude between the qBBr measurements reported in this study and those reported previously. Potententiometric titration measurement on *G. sulfurreducens* cells resulted in a calculated thiol concentration of 67.8 ± 22.8 µmol/gm wet weight (Figure 5b; Table 3). This value is in good agreement with our Hg EXAFS estimation of ~75 µM thiol sites/g wet weight cells, which is an indirect measurement of the abundance of thiols within the *G. sulfurreducens* cell envelope (Table 1).

4.0 Discussion

Complexation of Hg with high affinity thiol sites under low metal loading conditions, followed by binding of Hg to lower affinity carboxyl sites upon saturation of thiol sites has been documented previously (Mishra et al., 2011). Similar behavior has also been observed for Zn and Cd (Guiné et al. 2006; Mishra et al., 2010; Yu and Fein, 2015). Association of Hg with reduced S groups has also been shown in phytoplankton (diatoms) collected from a Hg contaminated creek using a combination of x-ray micro-fluorescence mapping and FTIR studies (Gu et al., 2014).

This study demonstrates that Hg complexation with intact bacterial cell suspensions, a mechanism which is likely applicable to other chalcophilic metals (e.g. Zn, Cd, and Pb) as well, is strongly dependent on metal loading and that the following conclusions can be drawn: 1) complexation of Hg with cell bound thiols is much more complicated than the formation of a single type of Hg-thiol complex at low Hg:biomass ratios; and 2) Hg can be complexed with cell-bound thiol sites in a variety of stoichiometries depending on the biogeochemical attributes of the ecosystem in question (e.g., the Hg:biomass ratio, the abundance of thiol sites on the bacterial species in question, and whether the species is Hg-methylating or not). It must be emphasized that in contrast with expectation from purely thermodynamic considerations, variation in the complexation behavior of Hg with thiols is not always dictated by the abundance of thiols on a given bacterial species.

Our results illustrate that *B. subtilis* and *S. oneidensis* MR-1 cells show similar Hg complexation behavior with cell bound thiols, albeit, the transition from Hg-S_2 to Hg-S_3 occurs at lower Hg loadings for *B. subtilis* due to lower thiol abundance compared to *S. oneidensis* MR-1. Although lower thiol concentrations in the case of *B. subtilis* prevented detailed examination of Hg-thiol interactions using Hg EXAFS below 0.5 µM Hg(II), as expected, *B. subtilis* formed Hg-S_2 and Hg-S_3 complexes at a lower Hg:biomass ratio than *S. oneidensis* MR-1.

While *B. subtilis* and *S. oneidensis* MR-1 exhibit the general trend outlined above, significant differences in Hg-thiol interactions were found between *G. sulfurreducens* and *S. oneidensis* MR-1 at low Hg(II) concentrations. In the case of *S. oneidensis* MR-1, Hg forms the Hg-S_3 complex below aqueous Hg concentrations of 0.5 µM, but forms Hg-S_2 and Hg-S complexes at higher Hg concentrations (Table 1). In contrast, under the same Hg concentration conditions, the Hg methylating species *G. sulfurreducens* forms only Hg-S_2 and Hg-S complexes without a detectable Hg-S_3 complex. This difference in surface complexation of Hg on the *G. sulfurreducens* cells was not caused by the lack of sufficient thiols on *G. sulfurreducens*. As shown above, *G. sulfurreducens* has the highest abundance of thiols among the three species examined. Although a definitive reason for the inconsistent behavior of *G. sulfurreducens* cell

envelope compared to those of *S. oneidensis* MR-1 and *B. subtilis* is beyond the scope of this study, these differences could provide insights about Hg cell surface complexes for methylating vs. non-methylating species. We hypothesize that the differences in the membrane protein chemistry (Hg transporters) and Hg uptake mechanism of *G. sulfurreducens* inhibits *G. sulfurreducens* to form Hg-S_3 type complexes unlike other two species examined. Our hypothesis is strengthened by a previous study which shows that aqueous Hg-S_2 complexes enhances Hg(II) uptake and subsequent methylation by *G. sulfurreducens* while aqueous Hg-S_3 complexes inhibit the same (Schaefer and Morel, 2009). In order to form Hg-S_3 complexes within cell envelopes, cell surface proteins must contain at least 3 thiol sites in close proximity to each other. Although *G. sulfurreducens* exhibits the highest concentration of thiols among the examined bacterial species, the thiol site density (i.e. sites/A^2) of *G. sulfurreducens* must not be high enough to make tridentate Hg-S_3 complex. These results suggest that the cell envelope S-amino acid containing proteins are significantly different between *G. sulfurreducens* and *S. oneidensis* MR-1, specifically their density and reactivity, which are critical in Hg binding, transport and possibly uptake. However, these results could be specific to a given bacterial species. Hence our results should not be generalized in the broader context of Hg-methylators vs. non-methylators without additional studies.

Differences in abundance and density of thiol sites on cells of different bacterial species, and the corresponding stoichiometry of Hg-thiol complexes that arise from those differences, could also explain the observed differences in passive oxidation of Hg(0) mediated by cell bound thiols (Colombo et al., 2014). These cell envelope bound Hg-S_n complexes also form readily in the presence of other strongly competing ligands, such as Cl^- and NOM (which also contains thiols), and were found to be stable in aqueous solutions at room temperature for over a period of 2 months (Figure S6; Dunham-Cheatham et al., 2014; Dunham-Cheatham et al., 2015). While the cell envelope-bound Hg-thiol complexes constitute the pool of Hg(II) transported inside the cell for Hg-methylation in the case of *G. sulfurreducens*, Hg-S_3 complexes in the non-methylating bacterial species *B. subtilis* and *S. oneidensis* MR-1 would likely stay as Hg-S_n complexes until the amino acid residue is oxidized. Given the high thermodynamic stability of Hg-S_3 complexes, they are not expected to be released back into the aqueous phase as thiol complexes. Alternatively, they could slowly transform into inorganic Hg-sulfide (e.g. meta-cinnabar) nanoparticles under sulfidic environments. It has been recently shown that Hg forms colloidal meta-cinnabar when reacted with DOM in the presence of sulfide, presumably via reaction with thiols in the DOM (Gerbig et al., 2011). It remains to be determined if thiols present within bacterial cell envelopes could also mediate the formation of meta-cinnabar, limiting the bioavailability of Hg for microbial processes (Zhang et al., 2012). Since bacteria are ubiquitous in all natural systems, and their cell envelope-bound reactive thiol site concentrations often exceed the aqueous concentrations of Hg in many natural and contaminated settings, this study suggests that cell envelope-bound thiol sites play a key role in the speciation, fate and bioavailability of Hg in aquatic and terrestrial ecosystems.

ACKNOWLEDGMENTS

The authors would like to dedicate this paper to the memory of Prof. Terry Beveridge, with whom collaborations began many years ago to investigate bacterial cell envelopes. The authors are grateful to Tamar Barkay and Francois Morel for their thoughtful discussions and comments. This work was funded by DOE-Subsurface Biogeochemical Research (SBR), and NSF (Chemical and Earth Sciences). BM was partially supported by the Argonne Subsurface Scientific Focus Area (SFA) project during the preparation of this manuscript, which is part of the SBR Program of the Office of Biological and Environmental Research (BER), U.S. DOE under contract DE-AC02-06CH11357. We are thankful to Jennifer Szymanowski and Madhavi Parikh for help with sample preparation, Dr(s). Tomohiro Shibata and Sayed Khalid for their help in beam line set-up and XAS measurements, and Dr. Jeffra Schaffer for helping with the cell cultures and insightful discussions.

627 **References**

628

629 1. Mergler, D.; Anderson, H. A.; Chan, L. H. M.; Mahaffey, K. R.; Murray, M.; Sakamoto, M.;
630 Stern, A. H.; Methylmercury exposure and health effects in humans: A worldwide concern.
631 *Ambio: J. Human Environ.*, **36**, 3-11 (2007)

632 2. Morel F.M.M.; Kraepiel, A.M.L.; Amyot, M.; The chemical cycle and bioaccumulation of
633 mercury, *Annu. Rev. Ecol. Syst*, , **29**, 543-566 (1998)

634 3. Barkay, T., & Schaefer, J.; Metal and radionuclide bioremediation: issues, considerations and
635 potentials. *Current opinion in microbiology*, **4**(3), 318-323. (2001)

636 4. Martell, A. E., & Smith, R. M. *Critical stability constants* (Vol. 1, p. 135). New York:
637 Plenum Press. (1974).

638

639 5. Carty, A. J., & Malone, S. F,. The chemistry of mercury in biological systems. *The*
640 *biogeochemistry of mercury in the environment*, **3**, 433-479. (1979)

641

642 6. Xia K., Skyllberg U.L., Bleam W.F., Bloor P.R., Nater E.A., Helmke P.A., X-ray absorption
643 spectroscopic evidence for the complexation of Hg(II) by reduced sulfur in soil humic
644 substances, *Environ. Sci. Technol*., **33**, 257-261 (1999)

645

646 7. Haitzer M., Aiken G.R., Ryan J.N., Binding of Hg(II) to dissolved organic matter: The role
647 of the mercury-to-DOM concentration ratio, *Environ. Sci. Technol*., **36**, 3564-3570 (2002)

648

649 8. Khwaja, A. R., P. R. Bloom, and P. L. Brezonik, Binding constants of divalent mercury
650 (Hg^{2+}) in soil humic acids and soil organic matter, *Environ. Sci. Technol*., **40**, 844– 849,
651 (2006)

652

653 9. Skyllberg, U., J. Qian, and W. Frech, Bonding of methyl mercury to thiol groups in soil and
654 aquatic organic matter, *Phys. Scr*., **T115**, 894– 896 (2005)

655

656 10. Skylberg Ulf, Competition among thiols and inorganic sulfides and polysulfides for Hg and
657 MeHg in wetland soils and sediments under suboxic conditions: Illumination of controversies
658 and implications for MeHg net production, *J. of Geophys. Res.*, **113,** (2008)

659

660 11. Nagy, K. L., Manceau, A., Gasper, J. D., Ryan, J. N., & Aiken, G. R., Metallothionein-like
661 multinuclear clusters of mercury (II) and sulfur in peat. *Environmental science & technology*,
662 **45**, 7298-7306. (2011)

663

664 12. Hesterberg, D., Chou, J.W., Hutchison, K.J., Sayers, D.E., Bonding of Hg(II) to reduced
665 organic sulfur in humic acid as affected by S/Hg ratio, *Environ. Sci. Technol*., **35**, 2741 –
666 2745 (2001)

667

668 13. Loux, N., An assessment of mercury-species-dependent binding with natural organic carbon,
669 *Chemical Speciation and Bioavailaibility*, **10**, 127-136 (1998)

14. Ravichandran, M., Interactions between mercury and dissolved organic matter – a review, *Chemosphere,* **55**, 319-331 (2004)

15. Skyllberg U., Bloom P.R., Qian J., Lin C.M., Bleam W.F., Complexation of mercury(II) in soil organic matter: EXAFS evidence for linear two-coordination with reduced sulfur groups, *Environ. Sci. Technol.,***40**, 4174-4180 (2006)

16. Schaefer Jeffra and Morel Francois, High methylation rates of mercury bound to cysteine by *Geobacter sulfurreducens*, *Nature Geoscience*, **2** (2009)

17. Schaefer, J. K., Rocks, S. S., Zheng, W., Liang, L. Y., Gu, B. H., Morel, F. M. M., Active transport, substrate specificity, and methylation of Hg(II) in anaerobic bacteria. *Proc. Natl. Acad. Sci*., **108**, 8714−8719 (2011)

18. Thomas, S.A., Tong, T. and Gaillard, J.F., Hg (II) bacterial biouptake: the role of anthropogenic and biogenic ligands present in solution and spectroscopic evidence of ligand exchange reactions at the cell surface. *Metallomics: integrated biometal science*, **6**(12), 2213-2222 (2014)

19. Lin, H., Lu, X., Liang, L. and Gu, B., Cysteine inhibits mercury methylation by Geobacter sulfurreducens PCA. *Environmental Science and Technology Letters*, **2**(5) (2005)

20. Mishra, B., O'Loughlin, E. J., Boyanov, M., Kemner K.M., Binding of Hg(II) to high-affinity sites on bacteria inhibits reduction to Hg(0) by mixed Fe(II/III) phases *Environ. Sci. Technol.* **45**, 9597-9603 (2011)

21. Colombo M.J., Ha J., Reinfelder J.R., Barkay T., Yee N., Anaerobic oxidation of Hg(0) and methylmercury formation by *Desulfovibrio desulfuricans ND132*. *Geochimica et Cosmochimica Acta* **112,** 166-177 (2013)

22. Hu, H., Lin, H., Zheng, W., Rao, B., Feng, X., Liang, L., Elias, D. A., and Gu, B., Mercury Reduction and Cell-Surface Adsorption by Geobacter sulfurreducens PCA, *Environ. Sci. Technol.,* **47**, 10922-10930 (2013)

23. Graham, A. M., Bullock, A. L., Maizel, A. C., Elias, D. A., and Gilmour, C. C., Detailed Assessment of the Kinetics of Hg-Cell Association, Hg Methylation, and Methylmercury Degradation in Several *Desulfovibrio* Species, *Appl. Environ. Microbiol*., **78**, 7337-7346 (2012)

24. Gu, B., Bian, Y., Miller, C.L., Dong, W., Jiang, X., Liang. L., Mercury reduction and complexation by natural organic matter in anoxic environments, *Proc. Nation. Acad. Sci.*, **108**, 1479-1483 (2011)

25. Zheng, W., Liang, L., Gu, B., Mercury Reduction and Oxidation by Reduced Natural Organic Matter in Anoxic Environments. *Environ. Sci. Technol*. **46**, 292–299. (2012)

26. Colombo M.J., Ha J., Reinfelder J.R., Barkay T., Yee N., Oxidation of Hg(0) to Hg(II) by Diverse Anaerobic Bacteria, *Chemical Geology*, **363**, 334-340 (2014)

27. Thomas, S.A. and Gaillard, J.F., Probing changes in Hg (II) coordination during its bacterial uptake. In *Journal of Physics: Conference Series* **712**(1), 12078-12081 (2016)

28. Borrok D., Aumend K. and Fein J. B., Significance of ternary bacteria-metall natural organic matter complexes determined through experimentation and chemical equilibrium modeling. *Chemical Geology*. **238**. 44-62 (2007)

29. Lovely, D.R. and Phillips, E.J.P., Novel mode of microbial energy metabolism: organic carbon oxidation coupled to dissimilatory reduction of iron or manganese. *Applied and Environmental Microbiology*. **54**. 1472-1480 (1988)

30. Fowle, D., and Fein, J.B. Experimental measurements of the reversibility of metal-bacteria adsorption reactions. *Chemical Geology***, 168**, 27-36 (2000)

31. Boyanov, M. I., S. D. Kelly, K. M. Kemner, B. A. Bunker, J. B. Fein, and D. A. Fowle. "Adsorption of cadmium to Bacillus subtilis bacterial cell walls: a pH-dependent X-ray absorption fine structure spectroscopy study." *Geochimica et Cosmochimica Acta* 67, no. 18 (2003): 3299-3311.

32. Claessens, Jacqueline, and Philippe Van Cappellen. "Competitive binding of Cu2+ and Zn2+ to live cells of Shewanella putrefaciens." *Environmental science & technology* 41, no. 3 (2007): 909-914.

33. Wei, Xing, Linchuan Fang, Peng Cai, Qiaoyun Huang, Hao Chen, Wei Liang, and Xinming Rong. "Influence of extracellular polymeric substances (EPS) on Cd adsorption by bacteria." *Environmental Pollution* 159, no. 5 (2011): 1369-1374.

34. Segre, C.U., Leyarovska, N.E., Chapman, L.D., Lavender, W.M., Plag, P.W., King, A.S., Kropf, A.J., Bunker, B.A., Kemner, K.M., Dutta, P. and Duran, R.S., The MRCAT insertion device beamline at the Advanced Photon Source. In *AIP Conference Proceedings*, **521**(1) 419-422 (2000).

35. Pasakarnis, T.S., Boyanov, M.I., Kemner, K.M., Mishra, B., O'Loughlin, E.J., Parkin, G. and Scherer, M.M., Influence of chloride and Fe (II) content on the reduction of Hg (II) by magnetite. *Environmental science & technology*, **47**(13), 6987-6994 (2013)

36. Dunham-Cheatham, S., Mishra, B., Myneni, S. C. B., Fein, J. B., The effect of natural organic matter on the adsorption of mercury to bacterial cells", *Geochimica et Cosmochimica Acta*, **150**, 1-10 (2015)

37. Dunham-Cheatham, S., Farrell, B., Mishra, B., Myneni, S., Fein, J. B., The effect of chloride on the adsorption of Hg onto three bacterial species", *Chemical Geology*, **373**, 106-114 (2014)

38 Joe-Wong C., Shoenfelt E., Jayne E., Crompton N., Myneni SCB. Determination of organic thiols in dissolved organic molecules and in bacterial cell membranes. *Environ. Sci. Technol.*, **46,** 9854-9861 (2012)

39. Yu, Q., Szymanowski, J., Myneni, S.C.B., and Fein, J.B., Characterization of sulfhydryl sites within bacterial cell envelopes using selective site-blocking and potentiometric titrations. *Chemical Geology*, **373,** 50-58.(2014)

40. Warner, T., and Jalilehvand, F., Formation of Hg (II) tetrathiolate complexes with cysteine at neutral pH. *Canadian journal of chemistry* **94**(4), 373-379 (2016)

41. Stern, E. A.; Newville, M.; Ravel, B.; Yacoby, Y.; Haskel, D. The UWXAFS analysis package - philosophy and details. *Phys. B*, **209**, 117–120 (1995)

42. Harris, H. H., Pickering, I. J., George, G. N., The Chemical Form of Mercury in Fish, *Science*, **301**, 1203 (2003)

43. Ravel, B.; Newville,M. ATHENA, ARTEMIS, HEPHAESTUS: Data analysis for x-ray absorption spectroscopy using IFEFFIT. *J. Synchrotron Radiat.* **12**, 537–541 (2005)

44. Richens, D. T., *The Chemistry of Aqua Ions*; Wiley: Chichester, (1997)

45. Almann, R., Structure of mercuric acetate, *Z. Kristallogr., Kristallgeom., Kristallphys., Kristallchem.* **138**: 366–373 (1973)

46. Manceau, A., and Nagy, K.L., Relationships between Hg(II)-S bond distance and Hg(II) coordination in thiolates, *Dalton Transactions*, **11**, 1421-1425 (2008)

47. Cheesman, B.V., Arnold, A.P. and Rabenstein, D.L., Nuclear magnetic resonance studies of the solution chemistry of metal complexes. 25. Hg (thiol) 3 complexes and Hg (II)-thiol ligand exchange kinetics. *Journal of the American Chemical Society*, **110**(19), 6359-6364 (1998)

48. Myneni SCB, Soft X-ray spectroscopy and spectromicroscopy studies of organic molecules in the environment, *Rev. in Mineral. and Geochem.*, **49**, 485-579 (2002)

49. Vairavamurthy A., Using X-ray absorption to probe sulfur oxidation states in complex molecules. *Spectrochimica Acta Part A- Mol. and Biomol. Spectr.*, **54**, 2009-2017 (1998)

50. Szilagyi, R.K. and Schwab, D.E., Sulfur K-edge X-ray absorption spectroscopy as an experimental probe for S-nitroso proteins, *Biochem. Biophys. Res. Commun.* **330**, 60-64 (2005)

51. Mishra, B., Boyanov, M., Bunker, B.A., Kelly, S.D., Kemner, K.M. and Fein, J.B., High-and low-affinity binding sites for Cd on the bacterial cell walls of Bacillus subtilis and Shewanella oneidensis. *Geochimica et Cosmochimica Acta*, **74**(15), 4219-4233 (2010)

52. Guiné, V., Spadini, L., Sarret, G., Muris, M., Delolme, C., Gaudet, J.P. and Martins, J.M.F., Zinc sorption to three gram-negative bacteria: combined titration, modeling, and EXAFS study. *Environmental science & technology*, *40*(6), pp.1806-1813 (2006)

53. Yu, Q., and Fein, J.B., The effect of metal loading on Cd adsorption onto *Shewanella oneidensis* bacterial cell envelopes: The role of sulfhydryl sites. Geochimica et Cosmochimica Acta **167**, 1-10 **(**2015)

54. Wei, J.; Saxena, A.; Song, B.; Ward, B. B.; Beveridge, T. J.; and Myneni, S. C. B.; Elucidation of functional groups on Gram-positive and Gram-negative bacterial surfaces using infrared spectroscopy, *Langmuir*, **20**, 11433–11442 (2004)

55. Rao, B., Simpson, C., Lin, H., Liang, L., Gu, B., Determination of thiol functional groups on bacteria and natural organic matter in environmental systems, *Talanta*, **119**, 240-247 (2014)

56. Xia, K., Weesner, F., Bleam, W.F., Bloom, P.R., Skyllberg, U.l., Helmke, P.A., XANES studies of oxidation states of sulfur in aquatic and soil humic substances. *Soil Sci. Soc. Amer. Journ.*, **62**, 1240-1246 (1998)

57. Risberg, E.D., Jalilehvand, F., Leung, B.O., Pettersson, L.G.M., Sandstrom, M., Theoretical and experimental sulfur K-edge X-ray absorption spectroscopic study of cysteine, cystine, homocysteine, penicillamine, methionine and methionine sulfoxide, *Dalton Transactions*, **12**, 3542-3558 (2009)

58. Gu, B., Mishra, B., Miller, C., Wang, W., Lai, B., Brooks, S.C., Kemner, K.M. and Liang, L., X-ray fluorescence mapping of mercury on suspended mineral particles and diatoms in a contaminated freshwater system. *Biogeosciences*, **11**(18), pp.5259-5267 (2014)

59. Gerbig, C. A., Kim, C. S., Stegemeier, J. P., Ryan, J. N., Aiken, G. R., Formation of Nanocolloidal Metacinnabar in Mercury-DOM-Sulfide Systems, *Environ. Sci. Technol.*, **45**, 9180-9187 (2011)

60. Zhang, T., Kim, B., Levard, C., Reinsch, B. C., Lowry, G. V., Deshusses, M. A., and Hsu-Kim, H., Methylation of Mercury by Bacteria Exposed to Dissolved, Nanoparticulate, and Microparticulate Mercuric Sulfides, *Environ. Sci. Technol.*, **46**, 6950-6958 (2012)

850

851 Table 1: Best fit values of Hg solution standards and Hg-biomass samples

Sample	path	N	R(Å)	σ^2 (10^{-3} Å^2)
Hg^{2+}	Hg-O	6.12 ± 0.65	2.30 ± 0.01	15.1 ± 3.5
HgAc	Hg-O	1.78 ± 0.32	2.06 ± 0.01	10.9 ± 0.9
	Hg-C	1.78[a]	2.83 ± 0.01	12.8 ± 4.0
Hg-cysteine	Hg-S	1.88 ± 0.21	2.32 ± 0.01	10.5 ± 1.2
*Hg-$(cysteine)_3$	Hg-S	2.82 ± 0.32	2.49 ± 0.01	13.5 ± 3.5
***Shewanella oneidensis* MR-1**				
350 µM	Hg-O	1.65 ± 0.25	2.06 ± 0.01	10.8 ± 1.5
	Hg-C	1.58 ± 0.32	3.05 ± 0.02	12.0 ± 3.8
100 µM	Hg-O	1.68 ± 0.24	2.06 ± 0.01	10.5 ± 1.2
	Hg-C	1.55 ± 0.28	3.05 ± 0.02	12.5 ± 3.5
50 µM	Hg-O	1.63 ± 0.15	2.06[b]	10.9[b]
	Hg-C	1.52 ± 0.35	3.05[b]	12.8[b]
	Hg-S	0.56 ± 0.12	2.32[c]	10.5[c]
25 µM	Hg-S	1.32 ± 0.21	2.31 ± 0.01	10.5 ± 1.5
15 µM	Hg-S	1.88 ± 0.18	2.32 ± 0.01	10.8 ± 1.3
5.0 µM	Hg-S	1.85 ± 0.19	2.35 ± 0.01	10.2 ± 1.2
2.5 µM	Hg-S	2.21 ± 0.28	2.44 ± 0.01	15.2 ± 3.0
0.5 µM	Hg-S	2.96 ± 0.25	2.51 ± 0.01	13.4 ± 2.5
Bacillus subtilis				
350 µM	Hg-O	1.62 ± 0.27	2.06 ± 0.01	10.8 ± 1.5
	Hg-C	1.52 ± 0.34	3.05 ± 0.02	12.0 ± 3.8
100 µM	Hg-O	1.65 ± 0.24	2.06 ± 0.01	10.5 ± 1.2
	Hg-C	1.58 ± 0.32	3.05 ± 0.02	12.5 ± 3.5
75 µM	Hg-O	1.22 ± 0.15	2.06 ± 0.01	10.9 ± 1.0
	Hg-C	1.15 ± 0.18	3.05 ± 0.01	12.8 ± 3.2

25 µM	Hg-O	1.65 ± 0.21	2.06[b]	10.5[b]
	Hg-C	1.82 ± 0.30	3.05[b]	12.8[b]
	Hg-S	0.42 ± 0.10	2.32 [c]	10.5 [c]
15 µM	Hg-O	1.58 ± 0.20	2.06[b]	10.5[b]
	Hg-C	2.02 ± 0.32	3.05[b]	12.8[b]
	Hg-S	0.61 ± 0.12	2.32 [c]	10.5 [c]
5.0 µM	Hg-S	1.80 ± 0.20	2.32 ± 0.01	10.2 ± 1.2
2.5 µM	Hg-S	1.95 ± 0.28	2.33 ± 0.01	10.5 ± 2.0
0.5 µM	Hg-S	2.26 ± 0.30	2.45 ± 0.01	10.9 ± 2.5
Geobacter Sulfurreducens				
75 µM	Hg-O	1.62 ± 0.18	2.06[b]	10.9[b]
	Hg-C	1.80 ± 0.21	3.05[b]	12.8[b]
	Hg-S	0.46 ± 0.14	2.32 [c]	10.5 [c]
25 µM	Hg-S	1.70 ± 0.21	2.32 ± 0.01	9.2 ± 1.3
15 µM	Hg-S	1.96 ± 0.18	2.32 ± 0.01	9.5 ± 1.7
5.0 µM	Hg-S	2.06 ± 0.19	2.36 ± 0.01	10.6 ± 2.8
2.5 µM	Hg-S	2.21 ± 0.28	2.38 ± 0.01	11.2 ± 3.0
0.5 µM	Hg-S	2.24 ± 0.22	2.38 ± 0.01	11.5 ± 3.6

*This standard is predominantly Hg-(cysteine)$_3$ but also contains Hg-(cysteine)$_4$

[a] Fixed this value to be the same as O based on crystallographic data.

[b] This was set to be equal to the HgAc standard.

[c] This was set to be equal to the Hg-cysteine standard.

Table 2: Values determined using qBBR measurements for surface thiol concentrations of *B. subtilis*, *S. oneidensis* MR-1, and *G. sulfurreducens* grown in the absence of Hg^{2+}. The error is one standard deviation.

Bacterial species	**µmoles thiols/ gram (wet mass)**	**Number of trails**	**wet:dry conversion**	**µmoles thiols/ gram (dry mass)**
B. subtilis	24±2	4	5.1	120±10
S. oneidensis MR-1	49±12	3	6.0	300±70
G. sulfurreducens	240±80	4	4.2	1000±300

Table 3. Summary of surface complexation modeling results for the potentiometric titrations of *G. sulfurreducens* with and without qBBr treatment. Five replicate titrations were conducted for each condition, and the values shown here represent the averages with 1σ uncertainties.

	pK_{a1}	C_1 µmol/g	pK_{a2}	C_2 µmol/g	pK_{a3}	C_3 µmol/g	pK_{a4}	C_4 µmol/g	C_{total} µmol/g
Untreated	3.2±0.2	192±36	5.2+0.1	104±7	7.2±0.2	41±3	9.5+0.2	69±20	406±24
qBBr-treated	3.4±0.4	139±36	5.2±0.1	94±10	7.0+0.0	44±6	9.3±0.1	62±10	338±46

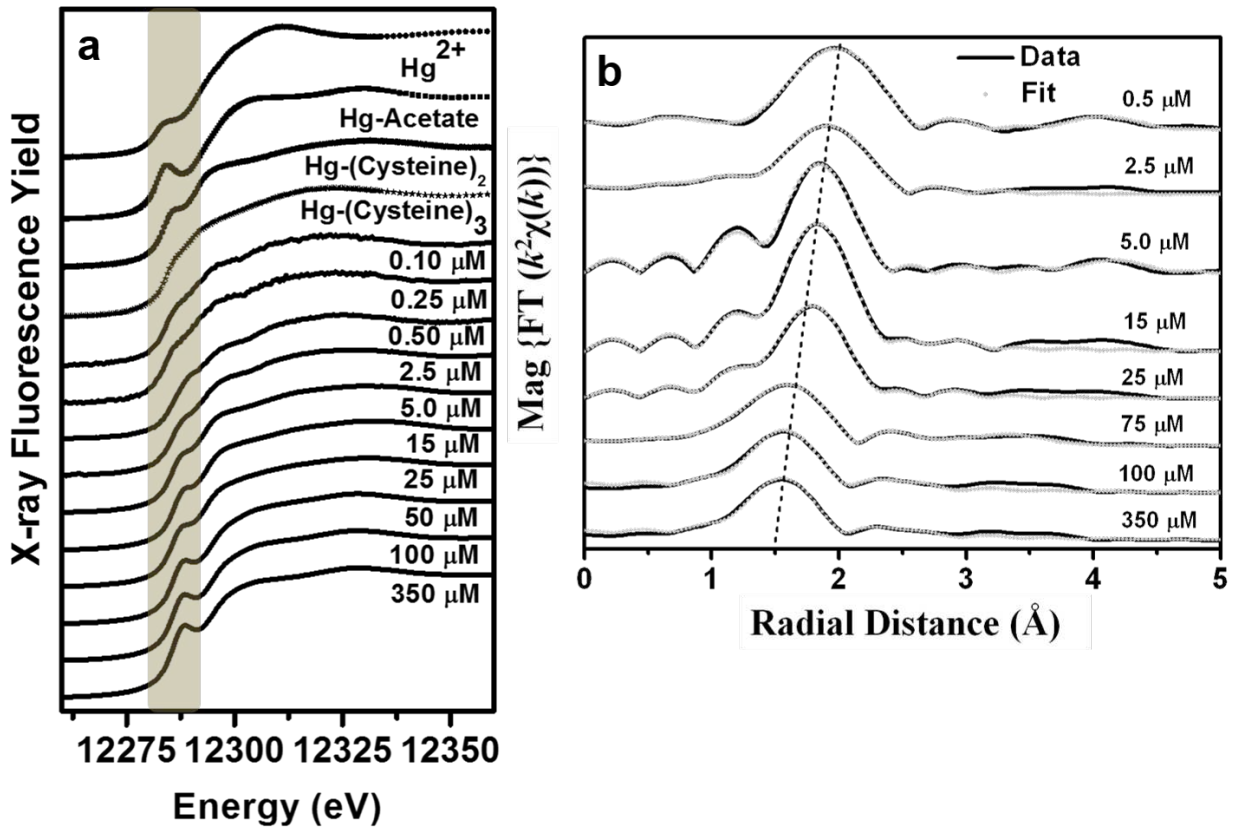

Figure 1. a) Hg L_3-edge XANES spectra of Hg^{2+} sorbed onto *S. oneidensis* MR-1 as a function of Hg^{2+} concentration. XANES spectra of model Hg-organic ligand complexes are also shown for comparison. b) Fourier transform mgnitude of Hg L_{III} edge EXAFS data and fits for Hg reacted *Shewanella oneidensis* MR-1.

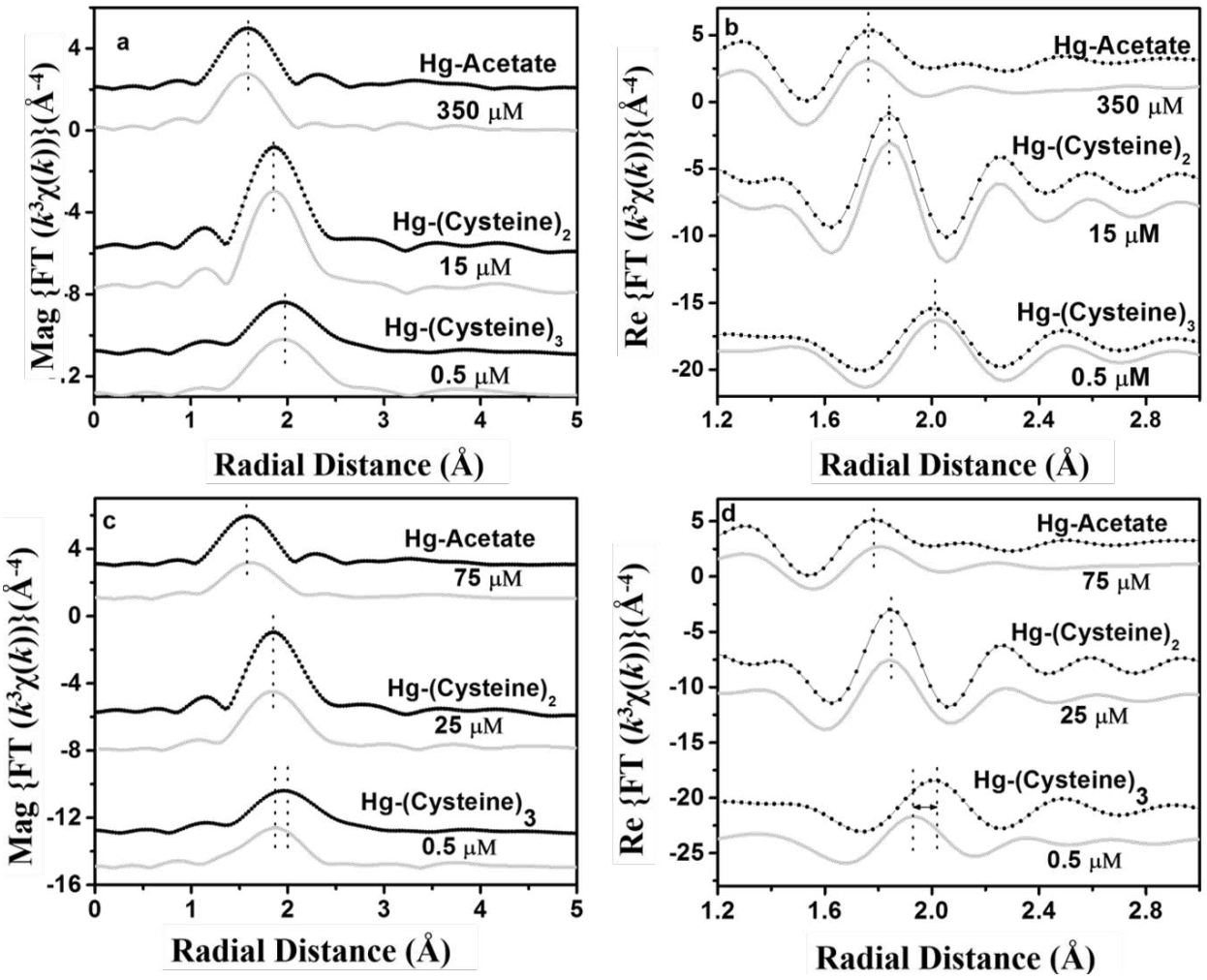

Figure 2. Structures of Hg complexes detected on cell envelopes of *S. oneidensis* MR-1 (top), and *G. sulfurreducens* (bottom). The spectra in "a" and "c" correspond to the Fourier Transform magnitude, and spectra in "b" and "d" correspond to the real part of Hg L_3 edge EXAFS spectra. Spectra of Hg-carboxylate, and Hg-cysteine are also included for comparison.

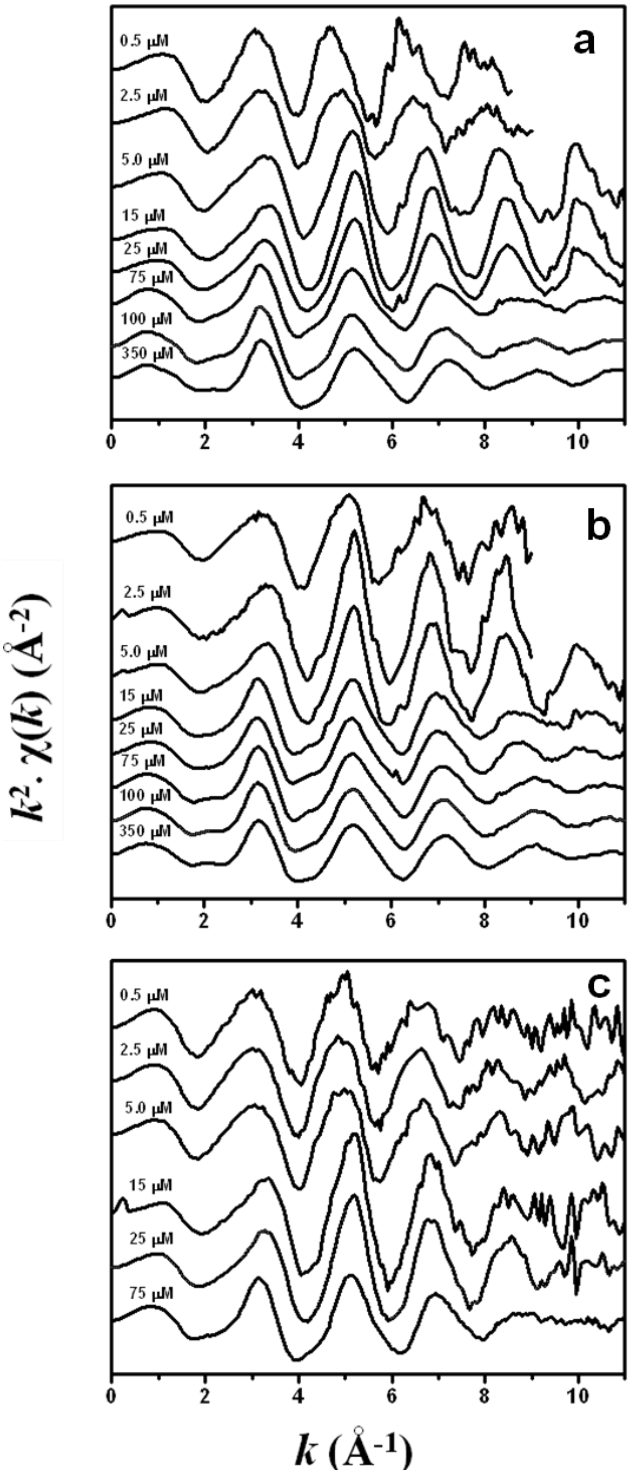

942
943
944 **Figure 3**: k^2 weighed $\chi(k)$ data for Hg L_{III} edge EXAFS
945 for a) *Shewanella oneidensis* MR-1, b) *Bacillus subtilis*,
946 and c) *Geobacter sulfurreducens*
947

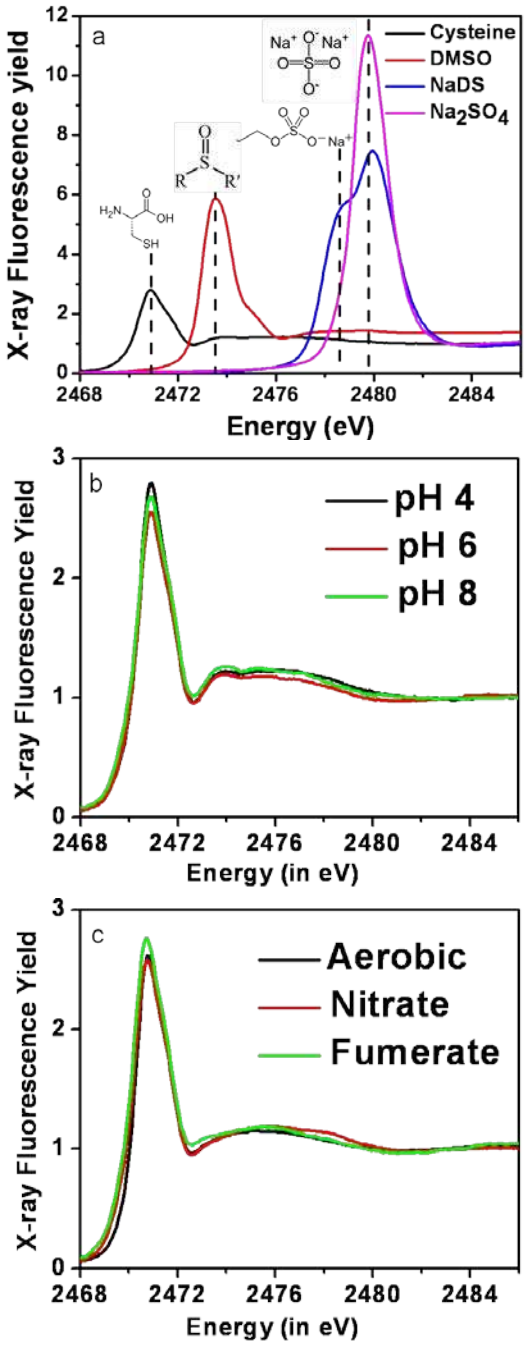

Figure 4: a) S K-edge XANES spectra of S standards (cysteine, dimethyl sulfoxide (DMSO), sodium dodecylsulfate (NaDS), and sodium laurel sulfate Na_2SO_4), b) S K-edge XANES on *S. oneidensis* MR-1 as a function of pH, and c) S K-edge XANES on *S. oneidensis* MR-1 cultured under different conditions.

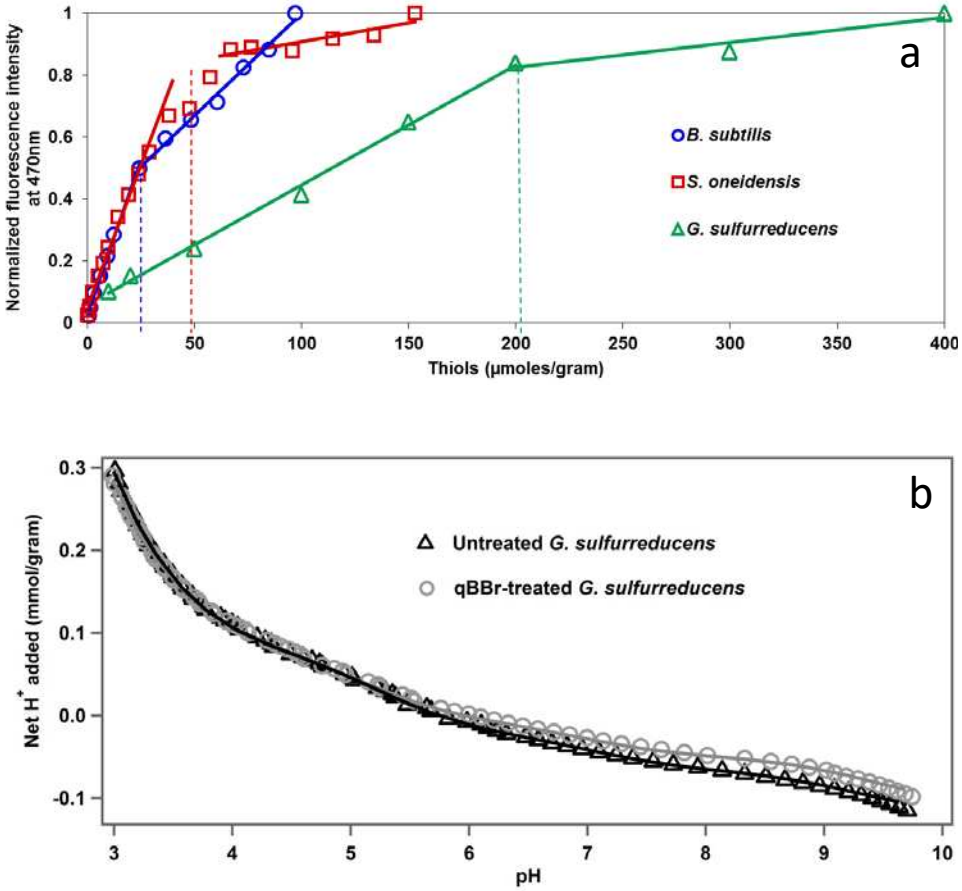

956

957

958 **Figure 5**. a) Concentration of reactive thiols on the cell envelopes of different bacterial species.
959 The dashed lines indicate the saturation concentration of fluorophore (or thiol) on each cell type.
960 b) Representative potentiometric titration curves of untreated and qBBr-treated *G.*
961 *sulfurreducens* suspensions (10g/L). Solid curves represent the best-fitting 4-site non-
962 electrostatic surface complexation models (SCM). Five replicate titrations were conducted both
963 with and without qBBr treatment, and the differences in calculated total site concentrations was
964 used to estimate the reported sulfhydryl concentrations (see Table 3).

965

966

967

968

969

970

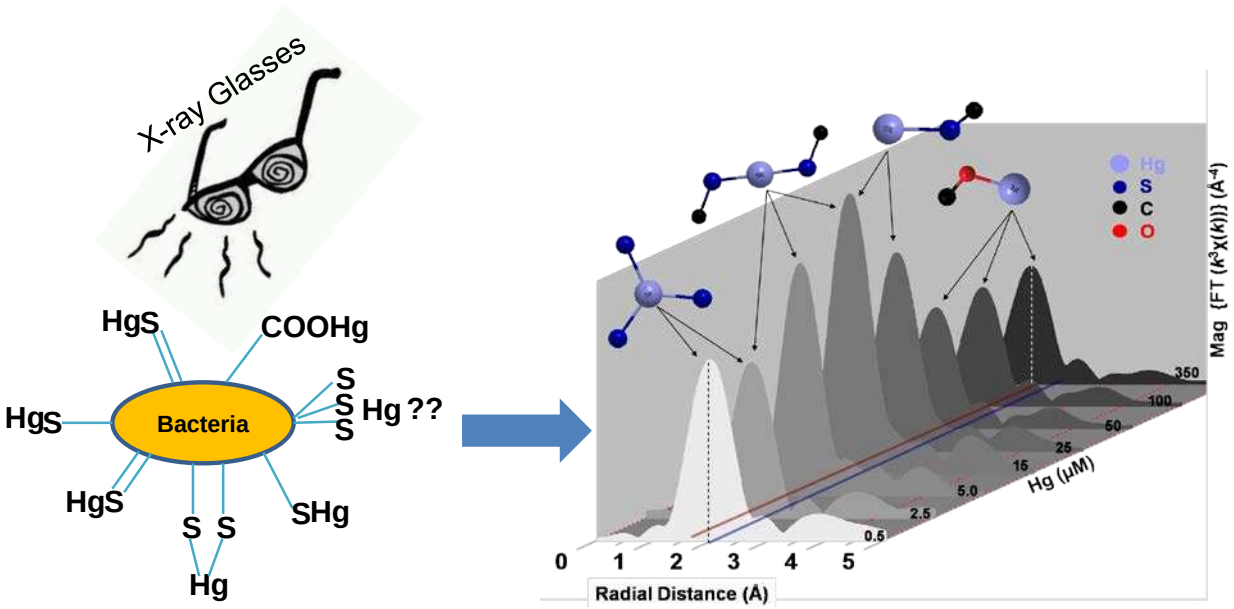

971

972

973

974 Artwork figure for optional graphical abstract

Supplementary Information

Stoichiometry of mercury-thiol complexes on bacterial cell envelopes

Bhoopesh Mishra[1*†], Elizabeth Shoenfelt[2], Qiang Yu[3], Nathan Yee[4],

Jeremy B. Fein[3], Satish C.B. Myneni[2*]

[1]Department of Physics, Illinois Institute of Technology, Chicago, Illinois, USA

[2]Department of Geosciences, Princeton University, Princeton, New Jersey, USA

[3]Department of Civil Engineering & Geological Sciences, University of Notre Dame, Notre Dame, Indiana, USA

[4]Department of Environmental Sciences, Rutgers University, New Brunswick, New Jersey, USA

[*]Co-corresponding authors. Email: (bmishra3@iit.edu); (smyneni@princeton.edu)

[†]Present address: School of Chemical and Process Engineering, University of Leeds, Leeds, UK.

Table S1: [Hg] adsorption by biomass samples determined using ICP-OES measurements.

B. subtilis		***S. oneidensis* MR-1**		***G. sulfurreducens***	
Initial Hg in solution (µM)	**Hg in supernatant (µM)**	**Initial Hg in solution (µM)**	**Hg in supernatant (µM)**	**Initial Hg in solution (µM)**	**Hg in supernatant (µM)**
0.04	ND*	0.06	ND*	0.05	ND*
0.11	ND*	0.14	ND*	0.15	ND*
0.21	ND*	0.20	ND*	0.24	ND*
0.43	ND*	0.45	ND*	0.52	ND*
1.07	ND*	1.12	ND*	1.2	ND*
2.15	0.10	2.10	0.08	2.76	0.12
4.26	0.15	4.55	0.12	5.20	0.21
12.93	0.21	13.10	0.18	15.01	0.45
21.49	1.26	21.60	0.62	25.23	1.16
53.32	3.58	55.7	2.86	75. 54	3.085
106.36	7.80	108.3	6.52	105.82	8.42
354.03	32.76	350.03	28.45	NA	NA

*Not detectable.

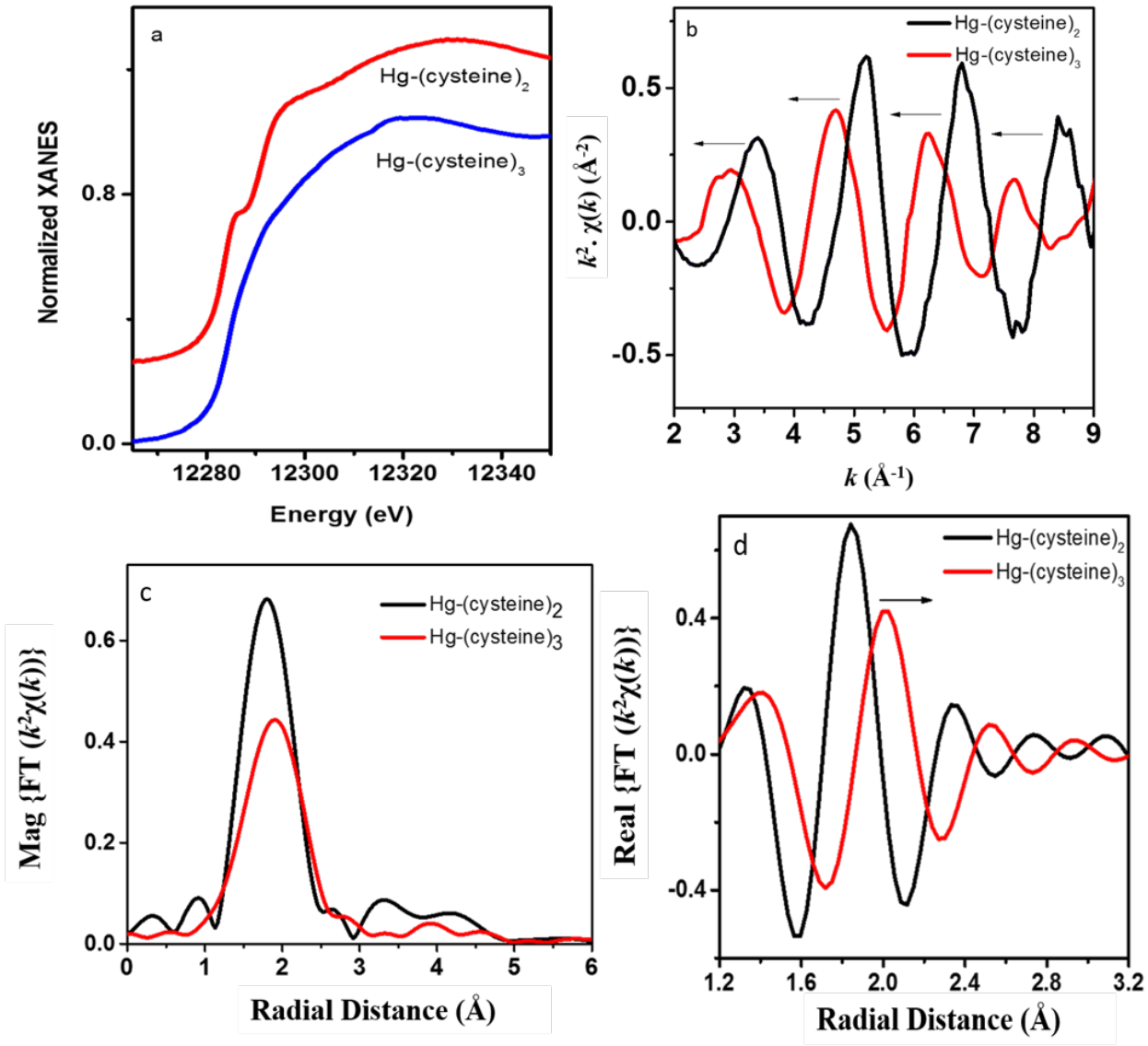

Figure S1: a) XANES, b) k^2 weighed $\chi(k)$ data, c) magnitude of EXAFS FT, and d) real part of the EXAFS FT data comparing Hg-(cysteine)$_2$ and Hg-(cysteine)$_3$ standards.

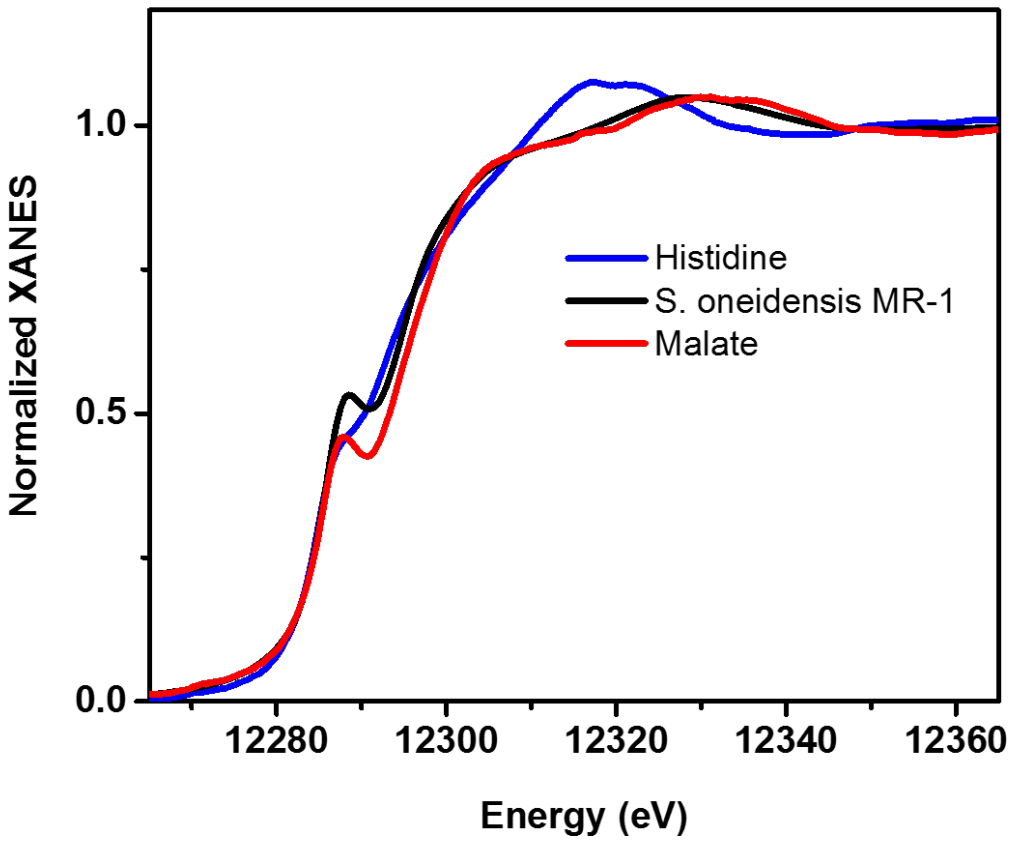

47

48 Figure S2: Comparison of Hg XANES spectra of Hg-histidine and Hg-malate aqueous complex
49 references with 75 µM Hg adsorbed to Shewanella oneidnensis MR-1 sample.

50

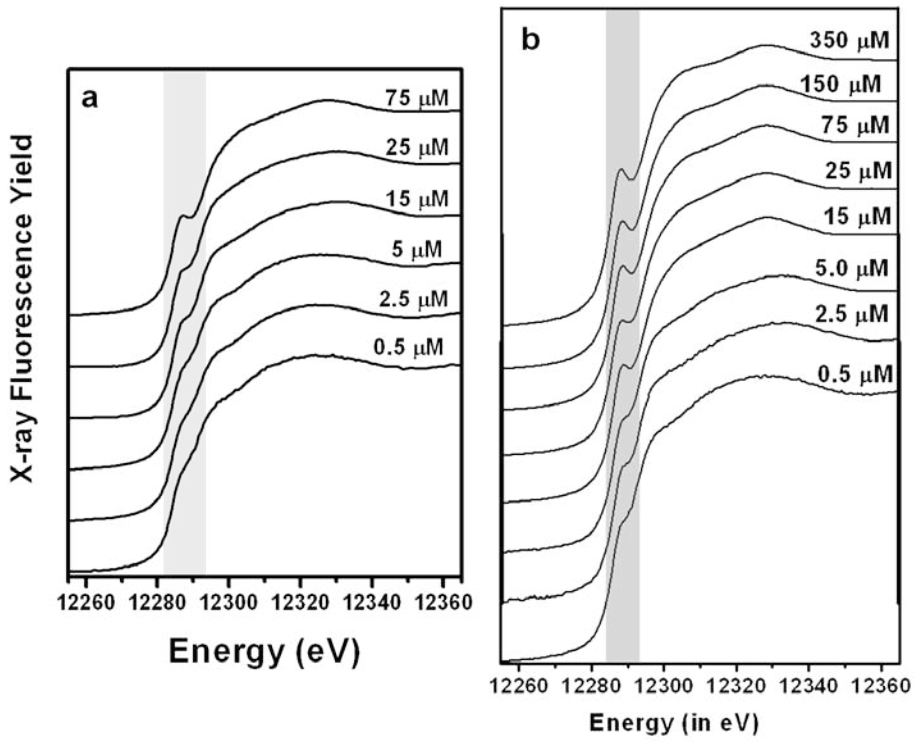

Figure S3: a) Hg L_{III} edge XANES for Hg reacted *Geobacter sulfurreducens* and b) *Bacillus subtilis* biomass samples.

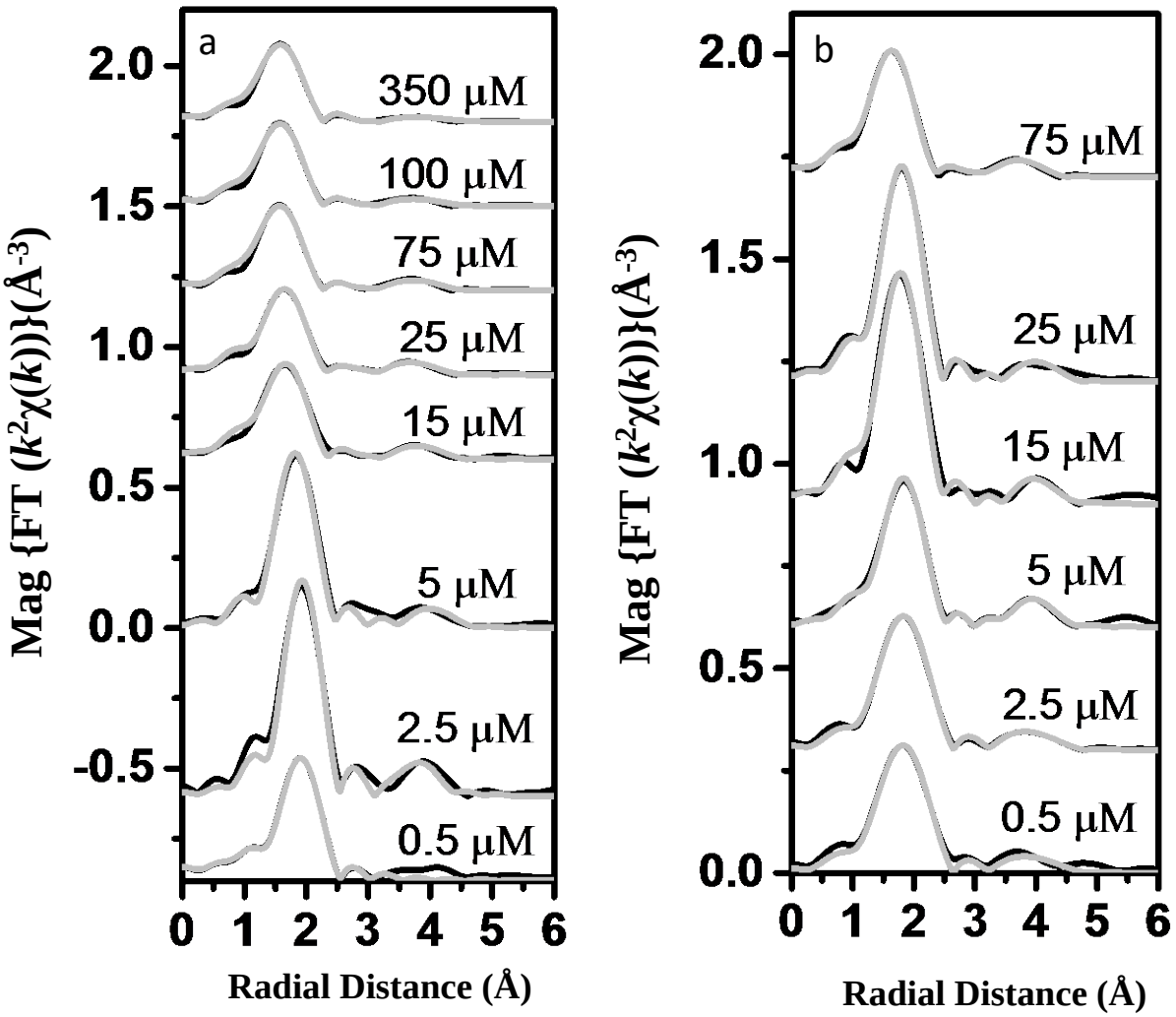

Figure S4: a) Hg L_{III} edge EXAFS FT magnitude data (solid black line) and fit (solid light grey line) for Hg reacted *Bacillus subtilis* and b) *Geobacter sulfurreducens* biomass samples.

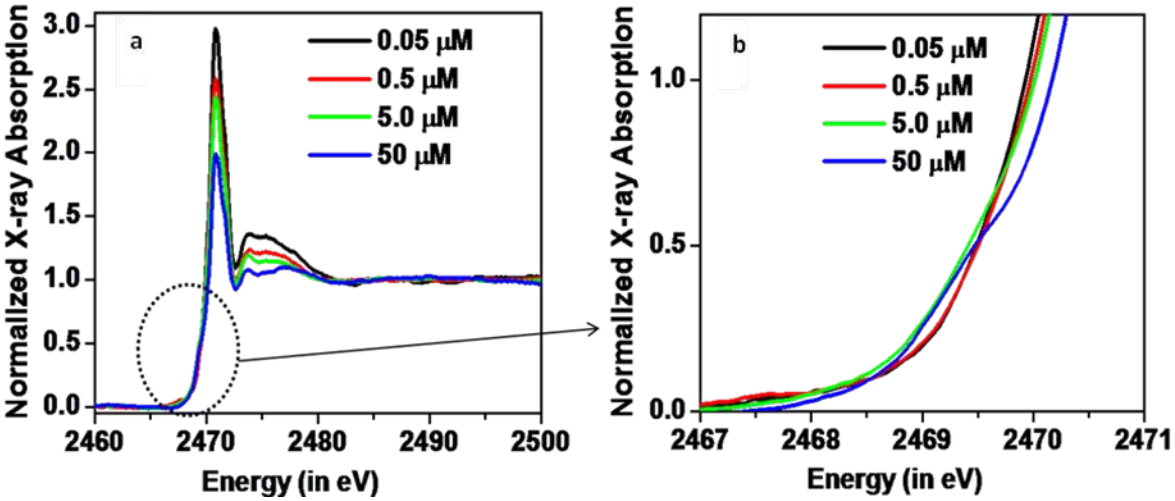

Figure S5**:** a) S K-edge XANES spectra of *S. oneidensis* MR-1 as a function of Hg concentration, and b) expanded pre-edge region (expanded for clarity) as a function of Hg loading on *S. oneidensis* MR-1 indicates the deprotonation of cysteine at higher Hg loadings.

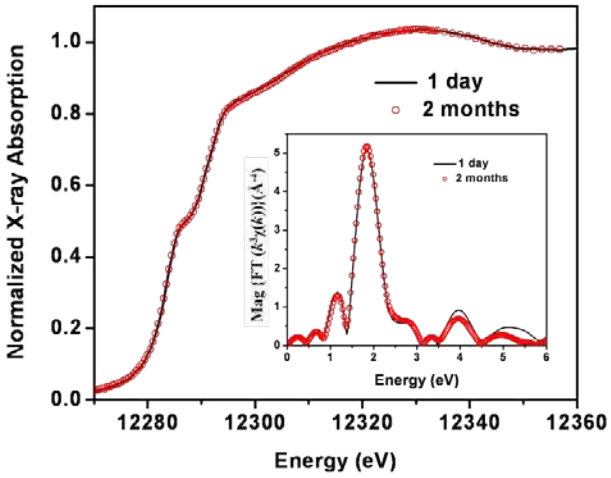

Figure S6: Hg L_{III} edge XANES on *Shewanella oneidensis* MR-1 reacted with 10 µM Hg^{II} for 1 day vs. 2 months. Inset shows corresponding Fourier transformed spectra.